Boundary Element Method Numerical Modeling: An Approach for Analyzing the Complex Geometry and Evolution of the San Gorgonio Knot, San Andreas Fault, Southern California

BOUNDARY ELEMENT METHOD NUMERICAL MODELING: AN APPROACH FOR ANALYZING THE COMPLEX GEOMETRY AND EVOLUTION OF THE SAN GORGONIO KNOT, SAN ANDREAS FAULT, SOUTHERN CALIFORNIA

A Thesis Presented
by
LAURA C. DAIR

Submitted to the Graduate School of the
University of Massachusetts Amherst in partial fulfillment
of the requirements for the degree of
MASTER OF SCIENCE
February 2009

GEOSCIENCES

BOUNDARY ELEMENT METHOD NUMERICAL MODELING: AN APPROACH FOR ANALYZING THE COMPLEX GEOMETRY AND EVOLUTION OF THE SAN GORGONIO KNOT, SAN ANDREAS FAULT, SOUTHERN CALIFORNIA.

A Thesis Presented
by
LAURA C. DAIR

Approved as to style and content by:

_____
Michele L. Cooke, Chair

_____
Laurie Brown, Member

_____
David F. Boutt, Member

_____
Michael Williams, Department Head
Department of Geosciences

ACKNOWLEDGEMENTS

I would like to thank my advisor, Michele L. Cooke, for all of her perfectly timed advice and patience. She has taught me a great deal and opened my eyes to many wonderful opportunities. I would also like to thank Scott Marshall who always had a well thought out method for every task.

I would like to thank the members of my committee, David F. Boutt and Laurie Brown for their wonderful support throughout my thesis work. I also wish to thank all of the members of the Research in Progress meeting who have helped me to make my thesis more clear, rounded, and accessible to a larger variety of geoscientists.

Funding for this research was provided by US Geological Survey National Earthquake Hazards Reduction Program grant #8HQGR0041 and a grant from Southern California Earthquake Center (SCEC). This manuscript is SCEC publication #1160. IGEOSS provided Poly3D modeling software and manipulation of fault surfaces was facilitated by use of 3DMove by Midland Valley Ltd.

ABSTRACT

BOUNDARY ELEMENT METHOD NUMERICAL MODELING: AN APPROACH FOR ANALYZING THE COMPLEX GEOMETRY AND EVOLUTION OF THE SAN GORGONIO KNOT, SAN ANDREAS FAULT, SOUTHERN CALIFORNIA.

FEBRUARY 2009

LAURA DAIR, B.A., SUNY GENESEO

M.A., UNIVERSITY OF MASSACHUSETTS AMHERST

Directed by: Professor Michele L. Cooke

The San Andreas fault forms the right lateral transform boundary between the North American and Pacific tectonic plates. At various locations along the San Andreas fault the geometry of the fault surface is much more complex than a straight, vertical, plane. The San Bernardino Mountain segment of the San Andreas fault, in the San Gorgonio Pass region has one of the most complex active fault geometries in southern California due to a left-stepping restraining bend in the San Andreas fault. The evolution of the actively faulting pass has created an intricate network of active and formerly active, dipping and vertical, three-dimensionally irregular fault surfaces. The purpose of this research is to gain a better understanding of the mechanics of the present day active fault geometry and the evolution in the San Gorgonio pass region, through numerical modeling. We use the three-dimensional Boundary Element Method modeling code Poly3D to simulate different fault configurations. We see that fault geometries that include geologically observed and inferred fault dips match geologic data more accurately than simplified, vertical faults in the San Gorgonio Pass region of the San Andreas fault. The evolution of the San Andreas Fault in the San Gorgonio Pass region

over the past million years may follow the principle of work minimization in the Earth's crust up until the present day configuration.

PREFACE

Chapter 1

We use the Boundary Element Method modeling code Poly3D to run our simulations of the San Andreas fault system in the San Gorgonio pass region. In chapter one we discus how Poly3D works and why Boundary Element Method modeling is used for this study.

Chapter 2

The first step of this research is to establish a geologically constrained present-day fault configuration for the primary San Andreas fault using numerical modeling. Establishing an accurate present day fault configuration could prevent the mischaracterization of seismic hazard. Net-slip distributions across three-dimensional, active fault surfaces produced by numerical models provide higher spatial resolution information than time averaged paleoseismic trench slip rates. This slip rate information can aid in hazard assessment earthquake prone areas. This section of the work is also used to validate the model.

Chapter two is presently in press at *Geology* and is therefore written with the plural first person. Very few changes have been made here to the in press manuscript, though some information on the modeling code and set-up have been added to keep the chapter consistent with the rest of the thesis.

Chapter 3

The second step is to determine whether or not the San Andreas fault system evolution has been governed by the principle of work minimization. Understanding how work minimization governs the mechanics of fault evolution may greatly improve

earthquake hazard assessment of the San Gorgonio Pass. Mechanical efficiency is use to analyze work minimization and is assessed using net slip along the faults and uplift of three different fault configurations from the last 500 Ka. Strain Energy Density is also analyzed to discover areas of potential fault propagation.

TABLE OF CONTENTS

ACKNOWLEDGEMENTS iii

ABSTRACT iv

PREFACE vi

LIST OF TABLES x

LIST OF FIGURES xi

CHAPTER

1. POLY3D 1

2. SAN ANDREAS GEOMETRY THROUGH THE SAN GORGONIO PASS, CALIFORNIA 4

Abstract 4
Introduction 4
Geologic Uplift and Slip Rates 6
San Andreas Model Alternatives 7
Model Configuration 8
Poly3D Modeling Method 9
Modeled Vertical Deformation Patterns 10
Site Specific Geologic Slip Rates 11
Slip Transfer: San Andreas Fault to San Jacinto Fault 11
Geomorphology and Regional Transpression 12
Preferred Fault Configuration 12
Conclusions 13

3. RECENT EVOLUTION OF THE SAN ANDREAS FAULT AT THE SAN GORGONIO KNOT, SOUTHERN CALIFORNIA 20

Abstract 20
Introduction 20
Geologic Background 22

Uplift of the San Bernardino Mountains 22
Present Day Fault Geometry and Slip Rates 23
Eastern California Shear Zone 26

Chronology of the San Andreas Fault Active Fault Geometry: Past 1 Ma 27
Numerical Investigations 28
Present Day Model Validation 29
Assessment of Mechanical Efficiency 32
Strain Energy Density Predicts Fracture Propagation 33
Evolution Model Set-Up 34
Modeled Average Net-slip 35
Modeled Uplift Pattern 37
Uplift analysis 38
Strain Energy Density 39

Strain Energy Density Analysis 40

Discussion and Implications 41

Missing Aspect 43

Conclusion 45

REFERENCES CITED 61

LIST OF TABLES

Table 3.1. Percent change with the addition of friction for Mill Creek and Present Day Models.. 47

LIST OF FIGURES

2.1. Fault trace map of the San Gorgonio Pass region. 15
2.2. Schematic drawing of the loading of the models. 16
2.3. Map view of the A) vertical, B) north-dipping SAF geometries. 17
2.4. Vertical deformation maps for both models. 18
2.5. Surface strike-slip rates along the fault traces within the San Gorgonio Pass region. 19
3.1. Area maps of the San Bernardino Mountain segment of the San Andreas fault in southern California. 48
3.2. A schematic drawing of the loading of the models 50
3.3. The modeled strike-slip distribution along the San Andreas fault (A), and San Jacinto fault (B) at the Earth's surface from the Cajon Pass to the Indio Hills. 51
3.4. Geologic versus Modeled uplift rates 54
3.5. The fault configurations taken from the CFM and extended to 35 km depth. 54
A) Shows the entire Mission Creek Configuration. 54
3.6. The weighted average net-slip. 55
3.7. Net-slip rates on secondary faults. 56
3.8. Vertical displacement maps. 57
3.9. Strain energy density maps for each of the model configurations. 58
3.10. A comparison of the Mill Creek and present day configuration. 59
3.11. Orientation changes of the San Gorgonio thrust surface trace. 60

CHAPTER 1

POLY3D

This study simulates the three-dimensional deformation of the San Andres fault system near the San Gorgonio Pass in southern California. The simulations are performed with Poly3D, a three dimensional Boundary Element Method (BEM) modeling code (Thomas, 1993). Poly3D solves for the deformation around fractures inside a linear elastic half-space using continuum mechanics, which assumes a continuous, isotropic, and homogeneous material. Crider and Pollard (1998) have shown Poly3D results are in good agreement with analytical solutions of linear elastic fracture mechanics. Faults in Poly3D are composed of multi-sided elements, each with a constant displacement discontinuity (Burger's vectors). On each element, you can prescribe either a Burger's vector or a traction for the dip, strike and opening directions. Prescribing a Burger's vector will cause the element to displace that amount. Prescribing a traction allows the element to slip until the tractions on the element equal the prescribed traction

With BEM, discretization only occurs along the faults, as compared to Finite Element Method (FEM) models. The principle of superposition allows the summation of the effects of multiple discrete forces, along the elements, for each point in the linear elastic half-space (Crouch and Starfield, 1990). In contrast to BEM, FEM requires that every point within a modeled volume reside within an element. Parameters can be assigned to each element of an FEM model volume making modeling heterogeneous materials, such as changes in rheology between stratagraphic layers, possible. Though FEM models may be able to simulate more complex properties, FEM models take much

longer to build and run then BEM models. BEM models cannot simulate complex properties but can simulate more complex geometries than FEM models. BEM models also contain less discretization, which means less discretization error (Crouch and Starfield, 1990). Because I am interested in investigating the effect of fault geometry, incorporating heterogeneous material is unnecessary.

The amount of strain applied to a Poly3D model, and hence the simulated time period is limited by the use of the infinitesimal strain conditions (i.e. < 1% strain) required with linear elastic fracture mechanics. Poly3D does a good job of describing deformation over short time periods (e.g. <5000 years) in the shallow crust where elastic deformation may dominate (e.g. Pollard et al., 2002; Griffith and Cooke, 2003; Muller and Aydin, 2003; Griffith and Cooke 2004; Olson and Cooke, 2005; Cooke and Marshall, 2006; Marshall et al., 2008). The triangular elements used in Poly3D are ideal for simulating the complex and irregular geometries characteristic of the active faults in the San Gorgonio Pass region. Fine meshes of triangular Poly3D elements have previously been used to simulate geologic deformation of complex fault configurations in the Los Angeles Basin (Griffith and Cooke, 2004; Griffith and Cooke, 2005; Cooke and Marshall, 2006; Meigs et al, 2008) and in the Ventura Basin (Marshall et al., 2008).

Within my models, the average diameter of elements along the San Andreas and San Jacinto faults is ~5 km and the element diameter decreases to ~2.5 km along the complex fault segments within the San Gorgonio Pass. The resolution of this mesh permits accurate simulation of varying slip distribution and deformation produced by fault irregularities as small as 10 km. Using the Sothern California Earthquake Center's

Community Fault Model (Plesch et al., 2007), a three-dimensional collection of the active and formerly active fault surfaces in southern California, I ensure that where faults intersect, the sides of elements line up and nodes are shared between two or more faults.

CHAPTER 2

SAN ANDREAS GEOMETRY THROUGH THE SAN GORGONIO PASS, CALIFORNIA

Abstract

Three-dimensional numerical models are needed to investigate the role of non-vertical strike-slip fault segments on the deformation within restraining bends. Numerical models simulate geologic deformation of two alternative three-dimensional present-day configurations for the San Andreas Fault (SAF) through the restraining bend within the San Gorgonio Pass region (SGPR) in southern California. Both models produce decreasing strike-slip rates southward along the San Bernardino strand of the SAF similar to geologic data. The north-dipping SAF model better matches the available strike-slip data as well as the geologic uplift data for the southern San Bernardino Mountains than the vertical SAF model. We conclude that a north-dipping fault configuration is preferred for models of the SAF in the SGPR. The complexity of the active fault geometry at the SGPR promotes the transfer of strike-slip from the SAF, to the nearby but unconnected San Jacinto fault. Slip rates and uplift patterns are sensitive to fault geometry within strike-slip restraining bends.

Introduction

Restraining bends along strike slip faults are traditionally believed to be composed of vertical strike-slip fault segments that curve along strike. However, two of the best-known restraining bends, the Santa Cruz and the San Bernardino Mountains (SBMs), California, may be associated with active non-vertical segments of the San

Andreas fault (e.g. Allen, 1957, Anderson, 1990; Matti et al., 1992; Nicholson, 1996; Yule and Sieh, 2003; Carena et al., 2004). As geophysical studies reveal greater details of active strike-slip fault geometry within restraining bends, we require three-dimensional models that can fully investigate the contribution of non-vertical strike-slip faults to local deformation.

At the San Gorgonio Pass region (SGPR) of southern California the San Andreas fault (SAF) steps left in a restraining bend that has evolved into a complex network of active and formerly active, dipping and vertical, three-dimensionally irregular fault surfaces (Figure 2.1; e.g., Matti et al. 1985). Although field and geophysical investigations reveal active north-dipping thrust faults through the SGPR (e.g., Allen, 1957, Matti et al., 1992; Nicholson, 1996; Yule and Sieh, 2003; Carena et al., 2004; Langenheim et al., 2005), crustal deformation and earthquake rupture models simplify the SAF as vertical through this region (e.g., Meade and Hager, 2005; Olsen et al., 2006; Smith and Sandwell, 2006). Within these simplified fault models, slip vectors are primarily strike-slip and the models neglect the reverse slip documented on the north-dipping San Gorgonio Thrust (Yule and Sieh, 2003). As a consequence, physical aspects of earthquake rupture dynamics and the regional seismic hazard may go uncharacterized. Models of the southern SAF with geologically realistic geometry, which are now possible at relatively high resolutions, may lead to more accurate assessment of earthquake hazards for southern California. Such models are of timely importance as the segments of the southern San Andreas Fault (SAF) south of the Cajon Pass have not slipped substantially enough to release accumulated strain and may be nearing the end of their recurrence intervals (e.g., Yule et al., 2001; Weldon et al., 2004; Weldon et al., 2005).

We use the Boundary Element Method (BEM) to numerically simulate geologic timescale crustal deformation of two different SAF configurations, through the SGPR. The BEM modeling technique uses a triangular mesh to accurately replicate three-dimensionally irregular fault surfaces. Using this mesh, we have developed the first crustal deformation model of the southern SAF that incorporates geologically constrained north-dipping fault segments. We compare the model results to geologic observations and offer a preferred fault configuration for the SAF through the restraining bend of the SGPR. Our study reveals the sensitivity of slip distribution and uplift pattern to fault configuration through a restraining bend and may guide future models in other regions.

Geologic Uplift and Slip Rates

The SGPR contains a complex network of strike-slip and thrust faults. Between the vertical strike-slip segments of the SAF north and south of the San Gorgonio Pass (i.e., the San Bernardino strand and Coachella Valley segment of the SAF), Yule and Sieh (2003) documented two active north dipping fault strands of the San Andreas, the San Gorgonio thrust (SGT) and the Garnet Hill fault (Figure 2.1). Microseismicity in the region suggests that these faults maintain their north dip of 45–85° at depth (Carena et al., 2004). Both the observed and interpreted north dip on these two faults refute the presence of a vertical through-going strand of the SAF within the SGPR (Figure 2.1; Yule and Sieh, 2003; Carena et al., 2004).

Low-temperature thermochronometry at the Yucaipa Ridge, located between the now inactive Mill Creek strand and the active San Bernardino strand of the SAF, indicates ~3–6 km of uplift in the last 1.8 My (Spotila et al., 2001). While the time averaged uplift rate of the Yucaipa Ridge is1.7 – 3.3 mm/yr, uplift was faster ca.1.5 Ma

than in the recent past (Spotila, et al., 2001). Offset markers across the SGT show 1 mm/yr relative uplift over the past 13 Ky (Yule and Sieh, 2003). Spatial variations in uplift rates are expected due to local fault geometry.

Geologic studies have revealed variable strike-slip rates along both the SAF and San Jacinto fault (SJF) within the SGPR Near the Cajon Pass, Weldon and Sieh (1985) found 24.5 ± 3.5 mm/yr strike-slip along the SAF Southward, rates decrease along the San Bernardino strand to 11 – 16 mm/yr at Badger Canyon (McGill et al., 2007) to 3 – 17 mm/yr at Plunge Creek (McGill et al., 2006), and to 2.6 – 7.0 mm/yr at Burro Flats (Orozco, 2004). Where the San Bernardino strand intersects the SGT and Garnet Hill strand of the SAF the strike-slip rate decreases to 5.7 ± 0.8 mm/yr (Yule and Sieh, 1997). The northern Coachella Valley segment of the SAF slips 9 – 15 mm/yr (Behr et al., 2007). Along the SJF, strike-slip rates vary from >20 mm/yr at site 7 (Figure 2.1; Kendrick et al., 2002) to >9.2 mm/yr from alluvial fan offsets (Rockwell et al., 1990). In addition to strike-slip rates in the region, Yule and Sieh (2003) found a minimum of 2.5 mm/yr reverse-slip on the SGT.

San Andreas Model Alternatives

Two different fault geometries for active faults in the SGPR were created based on the Southern California Earthquake Center Community Fault Model (CFM), a compilation of active faults in southern California (Plesch et al., 2007). The first model has a simplified vertical fault geometry for the SAF within the SGPR. The second model follows the preferred configuration of the CFM (Carena et al., 2004; Plesch et al., 2007) and includes a 45–85° north-dipping Garnet Hill strand and SGT (Figure 2.2B). In both models, the faults are freely-slipping to a depth of 35 km where they intersect a

horizontal freely-slipping crack that decouples crustal deformation from the modeled half space (Figure 2.3). The 35 km depth is chosen to match the imaged depth of the Mohorovičić discontinuity in this region (Magistrale et al., 2000). Within the model, discrete fault surfaces below the seismogenic crust simulate distributed deformation expected at these depths. Rather than prescribing slip along the faults within the SGPR, the weak faults of our model slip and interact in response to regional plate motions of 45 mm/yr N52°W right-lateral displacement (e.g. Bennett et al, 1999; Shen et al., 2003) applied at the edges of the horizontal crack.

Model Configuration

The models include the Mojave segment and the Coachella Valley segment of the San Andreas fault, as well as the San Jacinto Valley strand and the Anza segment of the San Jacinto fault. The San Gorgonio Pass region is comprised a complex array of formerly and presently active faults. For this model we focused on faults that exhibit significant recent activity. For example, the western portion of the mapped San Gorgonio thrust was not included in the model due to lack of recent activity. The San Bernardino strand of the San Andreas fault was included in the model because paleoseismicity shows this fault to be one of the major strands through the pass (Weldon and Sieh, 1985; McGill et al., 2007; McGill et al., 2002; Orozco, 2004). Subtle pressure ridges and hanging walls near the southern most surface trace of the San Bernardino strand suggest that the fault merges with the eastern portion of the San Gorgonio thrust (Yule and Sieh, 2003). Within the model, the San Gorgonio thrust has a north dip of 45-70˚, and merges to the east with the Garnet Hill strand of the San Andreas Fault. The Garnet Hill strand dips to the north at 55-85˚, and parallels the Banning strand. Both the Garnet hill and the Banning faults

are believed to be active north of Palm Springs. For simplicity, we only include the Garnet Hill strand to represent deformation on both of these active parallel fault strands. Seismicity indicates that the Garnet Hill strand of the San Andreas fault extends from the San Gorgonio thrust to the Coachella Valley segment of the San Andreas fault even though geologic mapping does not show a surface trace intersection between the two faults (Langenheim et al., 2005). All of the three-dimensional faults included in the models have been smoothed at depth to remove any small irregularities observed along the fault trace at the Earth's surface that are unlikely to extend to significant depths.

Though the San Jacinto is made up of many en echelon faults (Sharp 1975), our models consider the fault to be continuous and connected. Delineating the San Jacinto fault into individual echelon strands may decrease the strike-slip rates on the San Jacinto fault but is not expected to substantially change the slip rates along the San Andreas fault strands within the San Gorgonio Pass region.

Poly3D Modeling Method

The models are run using Poly3D, a three dimensional Boundary Element Method (BEM) modeling code (Thomas, 1993). For this study, the BEM code is used to simulate the three-dimensional active faulting near the San Gorgonio Pass inside a linear elastic half-space. The triangular elements used in Poly3D are ideal for complex geometries characteristic of the active faults in the San Gorgonio Pass region. Fine meshes of triangular Poly3D elements have previously been used to simulate geologic deformation in the Los Angeles Basin (Griffith and Cooke, 2004; Griffith and Cooke, 2005; Cooke and Marshall, 2006; Meigs et al, 2008) and in the Ventura Basin (Marshall et al., in press). Within our models, the average diameter of elements along the San Andreas and

San Jacinto faults is ~5 km and the element diameter decreases to ~2.5 km along the complex fault segments within the San Gorgonio Pass. The detail of this mesh permits accurate simulation of fault irregularities larger than 10 km.

Modeled Vertical Deformation Patterns

The surface uplift maps reveal significant differences between the vertical and north-dipping SAF models (Figure 2.4). The vertical configuration produces far less relative surface uplift than the north-dipping configuration. The greater uplift rates on the hanging wall of the north dipping SAF model are due to significant reverse slip rates on the dipping fault segments. The average reverse slip rate on the modeled SGT, 3.6 mm/yr, matches geologic observations (>2.5 mm/yr; Yule and Sieh, 2003). The north-dipping model has the greatest relative uplift in the areas of the Yucaipa Ridge block and the Morongo block (Figure 2.1), which have been uplifted at higher rates than the surrounding area (Spotila et al., 2001). The relative uplift rates produced by the north-dipping fault model at the Yucaipa Ridge (~1.6–1.9 mm/yr) fall within the lower half of time averaged geologic uplift rates, (1.6–3.3 mm/yr), which is also consistent with slower uplift in times later than 1.5 Ma (Spotila et al., 2001). In contrast, the vertical fault model produces only ~0.4–0.7 mm/yr of relative uplift and cannot account for the geologic uplift rates. Vertical models with strike-slip rates as fast as 28 mm/yr though the restraining bend can produce 1–3 mm/yr of uplift adjacent to the fault (Smith and Sandwell, 2003); however such slip-rates greatly exceed the geologic observations within the restraining bend in the SGPR (Figure 2.5). Both of our models produce subsidence >1 mm/yr within the San Bernardino Basin, which is consistent with depositional rates of ~1 mm/yr in this valley (Matti and Morton, 1993).

Site Specific Geologic Slip Rates

We also compare the modeled slip rates at the Earth's surface with geologic rates obtained through specific paleoseismic and geomorphic studies (Figure 2.5). The modeled strike-slip rates along the San Bernardino strand of the SAF decrease to the southeast and correlate well with geologic slip rates. However, the vertical SAF model overestimates right-lateral slip rates at more sites along the San Bernardino strand of the SAF than the north-dipping model. Again, the north-dipping fault configuration shows a more favorable comparison to geologic observations than the vertical fault model. The strike slip rate data along the SJF cannot distinguish between the models due to the simplification of the modeled SJF.

The geologically observed, and model reproduced pattern of decreasing slip rate to the southeast along the San Bernardino strand of the SAF, demonstrates the significant spatial variability of slip rates along fault segments due to interaction with nearby faults. The discrepancy of some geologic slip rates on the San Bernardino fault segment with slip rates from geodetic block models (Meade and Hager, 2005) may reflect the inability of the block models to incorporate the region's geologic complexity.

Slip Transfer: San Andreas Fault to San Jacinto Fault

Right-lateral slip along the SAF is lowest for both models along the SGT/Garnet Hill strand, which is the area of greatest geometric complexity. This decrease in strike-slip rate along the SAF occurs at the same distance from the Cajon Pass as the greatest strike-slip rates along the SJF (Figure 2.5). This suggests that, in the model, strike-slip is transferred from the SAF to the SJF even though the faults are not hard-linked (connected). Within the models, the inefficiency of the restraining bend impedes strike-

slip along the SAF allowing the SJF to absorb the excess strike-slip (Figure 2.5). Slip can transfer between two separated faults as the shear stresses are transmitted through the intervening material producing a soft-link (e.g., Crider and Pollard, 1998; Roberts and Michetti, 2004). When slip cannot be accommodated on a fault due to an inefficient geometry, some of that slip is taken up by other faults and the remainder becomes off fault deformation.

Geomorphology and Regional Transpression

Although deformation is driven by N52°W right-lateral displacements at the edges of the model, the lack of applied *regional* transpression does not hinder the development of localized uplift in the north-dipping model. The contrasting uplift produced by the vertical and north-dipping SAF models indicates that dipping fault geometry can account for significant uplift without regional transpression. The inference that local fault configuration contributes to SBMuplift is consistent with the conclusions of several uplift studies in the region (e.g., Dibblee, 1975; Matti and Morton 1993; Spotila and Sieh, 2000; Spotila et al., 2007).

Preferred Fault Configuration

The vertical SAF model fails to match the geologic uplift pattern, overestimates slip rates at several sites along the San Bernardino strand of the SAF, and neglects the geologic and seismic indications of active north-dipping faults in the SGPR. Of the two models, we favor the north-dipping geometry for the San Andreas Fault through the SGPR.

Our results suggest that crustal deformation models for restraining bends that use only vertical faults will overestimate slip rates and underestimate off-fault deformation. The complexity of active faults through the SGPR may influence earthquake rupture scenarios because regions of fault surface complexity may be regions where ruptures initiate, terminate, or jump to other faults (e.g., Harris et al., 1991; Wald and Heaton, 1994). Earthquake rupture along the southern SAF may produce significant ground shaking within the metropolitan Los Angeles region (Olsen et al., 2006). Consequently, the constraints on fault geometry suggested here will help future rupture models of the southern SAF more accurately predict seismic hazards.

Conclusions

Our, three-dimensional models confirm the geologic and geophysical evidence for north –dipping active fault segments along the SAF within the SGPR and demonstrate that non-vertical strike-slip segments can play a significant role in active deformation of restraining bends. Furthermore, incorporating geologic complexities, such as dipping fault surfaces, into numerical fault models, which is now more feasible then ever, increases the match between modeled results and geologic observations. For example, the uplift of the SMBs is better matched by active north-dipping faults within the restraining bend than by a vertical SAF. Similarly, the north-dipping SAF model better matches variable strike-slip rates at sites along the San Bernardino strand of the SAF. The match of the model results to the geologic observation of decreasing strike-slip along the San Bernardino strand of the SAF highlights the value of geologic timescale models that do not prescribe fault slip rates a priori. Within the models of the SGPR, the SJF picks up some of the strike slip that is lost to the SAF in an effort to by-pass the inefficient SAF

geometry. This transfer occurs between soft-linked faults that have no physical connection. This study also reveals the sensitivity of uplift patterns and fault slip rates to fault geometry within restraining bends. Our results highlight the need for crustal deformation models of restraining bends to carefully consider non-vertical strike-slip fault geometry.

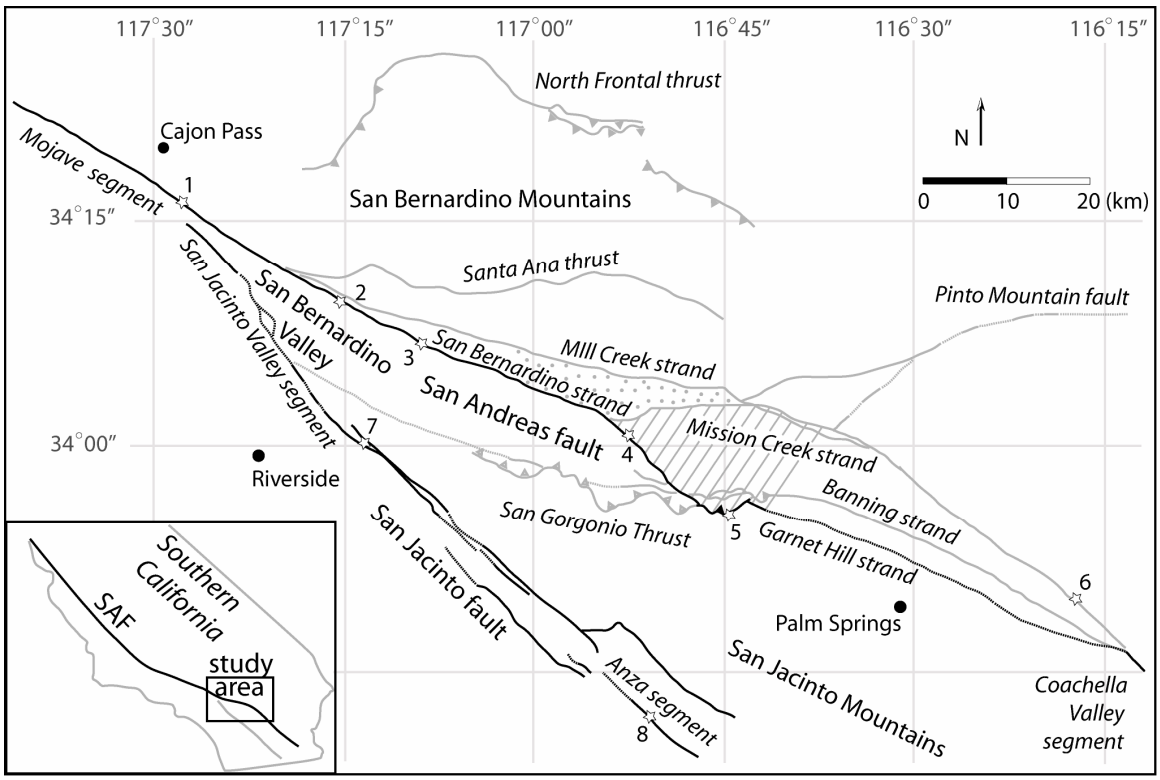

Figure 2.1. Fault trace map of the San Gorgonio Pass region. Model simulations of active faulting only include the black faults. The gray faults are secondary. Stars indicate locations of geologic study sites that have yielded slip rates. The dashed lines indicate faults that have no surface trace. The stippled section is the Yucaipa Ridge block while the cross-hatched section is the Morongo Block of the San Bernardino Mountains. Site 1, Cajon Pass– Weldon and Sieh, 1985; site 2, Badger Canyon– McGill, 2007; site 3, Plunge Creek- McGill et al., 2006; site 4, Burro Flats – Orozco, 2004; site 5, Yule et al., 2001; site 6 - Behr et al., 2007; site 7 - Kendrick et al., 2002; site 8 - Rockwell et al., 1990 and Rockwell, 2006 (modified from Matti et al., 1992).

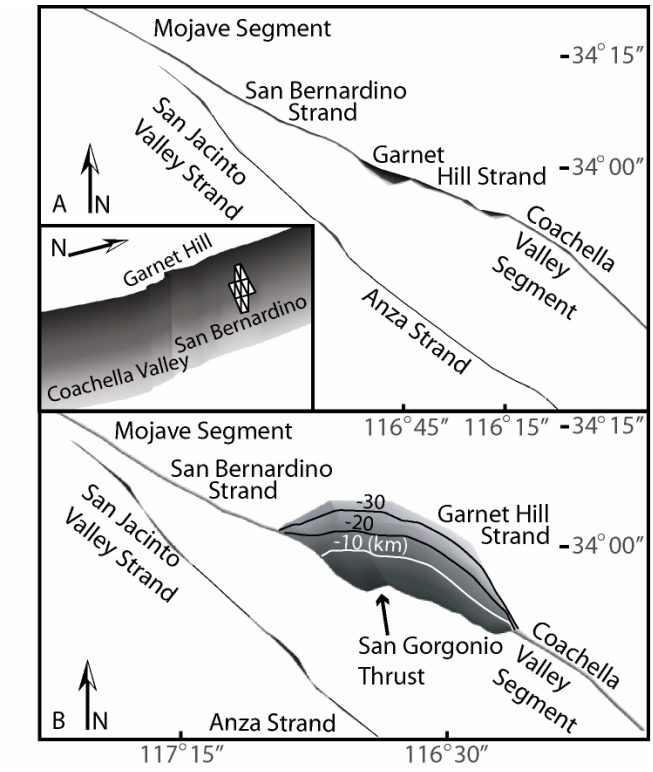

Figure 2.1. Schematic drawing of the loading of the models. The edges of the 35 km deep detachment as well as the distal tips of the primary faults have prescribed slip. The slip on the detachment is decreased incrementally as each section nears the strike-slip fault until slip on the section adjacent to the fault matches the prescribed slip on the fault tip. Away from the model boundaries all faults slip and interact in response to the loading at the edges.

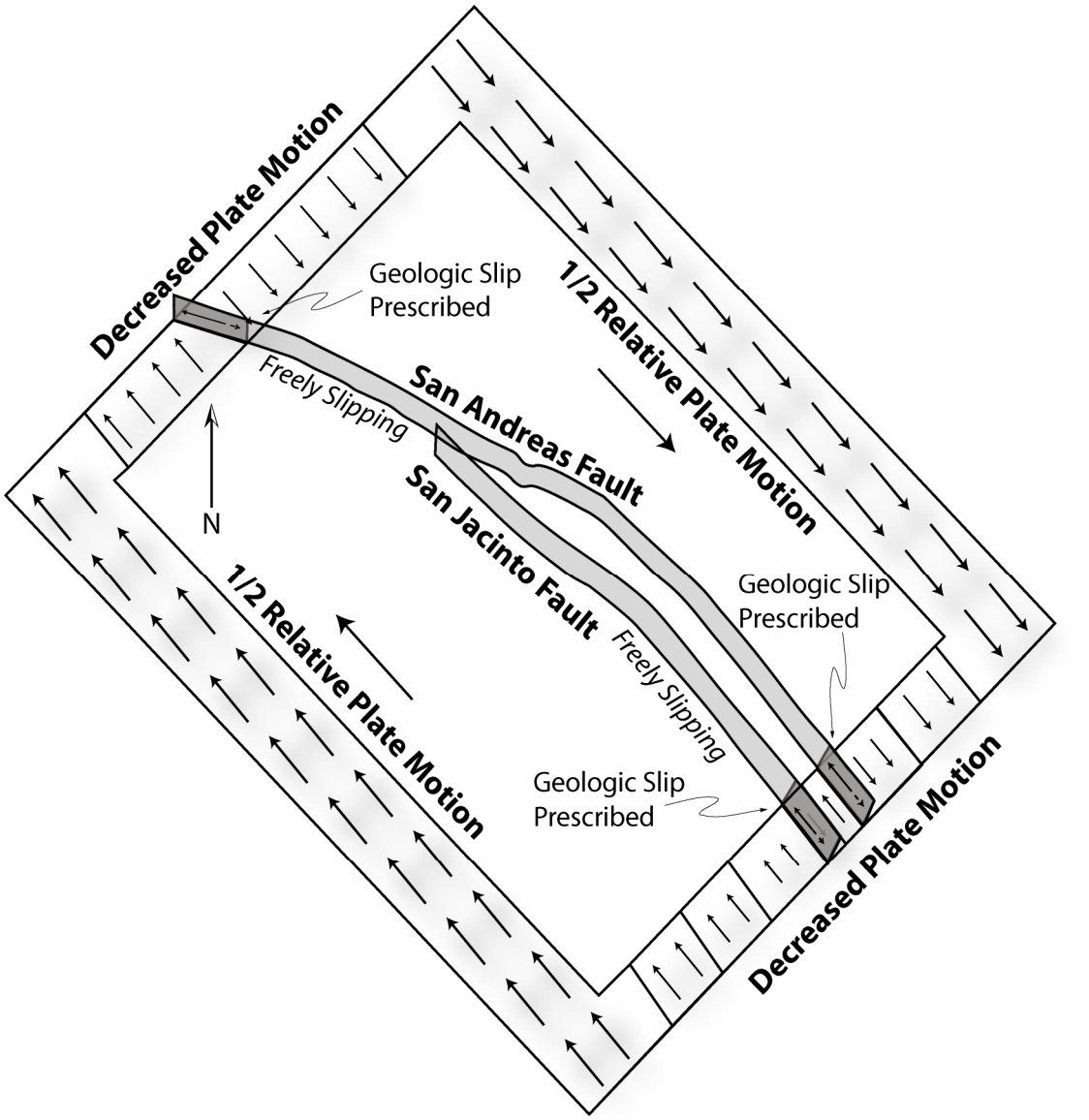

Figure 2.2. Map view of the A) vertical, B) north-dipping SAF geometries. Lighter shades indicate deepening depths to 35 km. Structure contours are overlain on dipping segments. The inset within A) shows a section of the mesh used for the fault surfaces.

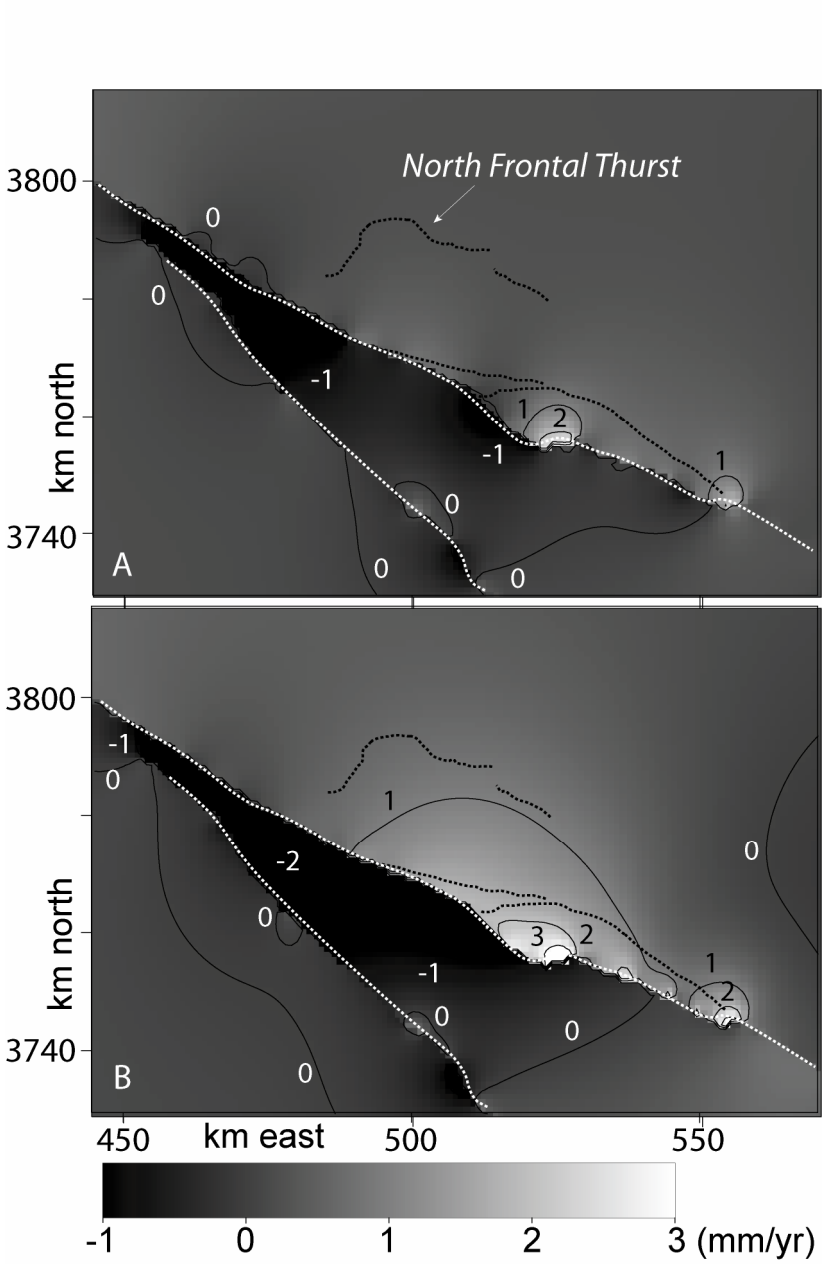

Figure 2.3. Vertical deformation maps for both models. Unlike the vertical model, the dipping models produce uplift within the region of the southern San Bernardino Mountains (e.g., the Yucaipa Ridge and Morongo Blocks (Figure 2.1). The dotted lines are faults (Figure 2.1).

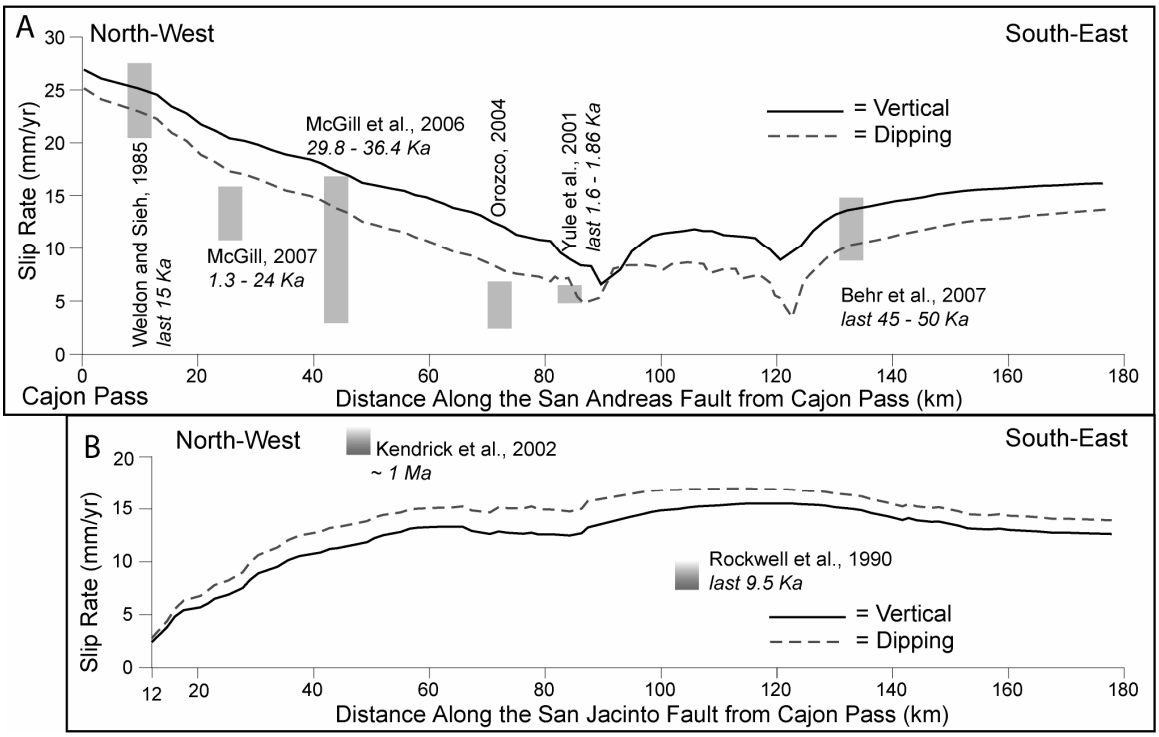

Figure 2.4. Surface strike-slip rates along the fault traces within the San Gorgonio Pass region. The graphs have been arranged so that the scales are the same and positioned according to distance from Cajon Pass. The northwestern half of plot A shows decreasing strike-slip rate along the San Bernardino strand of the San Andreas fault from Cajon Pass to the San Gorgonio thrust. The vertical, continuous model has the greater right-lateral slip rate along the San Andreas fault and exceeds geologic slip rates at more sites than the north-dipping model. The vertical San Andreas fault model has slower strike-slip rates than the north-dipping model along the San Jacinto fault in graph B. The gradational ranges indicate minimum slip rate estimates.

CHAPTER 3

RECENT EVOLUTION OF THE SAN ANDREAS FAULT AT THE SAN GORGONIO KNOT, SOUTHERN CALIFORNIA

Abstract

During the last 500 ka the San Andreas fault within the San Gorgonio Pass region has been active along three different fault configurations; the Mission Creek fault configuration (>500 kya), the Mill Creek fault configuration (500-125 kya), and the present day fault configuration (< 125 kya). Three-dimensional numerical models are used to test the hypothesis that fault systems evolve to increase mechanical efficiency. The present day model configuration matches geologic slip rate and uplift rate data well, which supports the utility of numerical modeling for understanding geologic deformation. Three-dimensional Boundary Element Method simulations of each of the three fault configurations produce uplift patterns and net-slip that reveal the mechanical efficiency of the system. Mechanical efficiency increases from the Mission Creek to Mill Creek fault configuration and decreases from the Mill Creek configuration to the present day configuration. Strain energy density patterns highlight regions of possible fault propagation and may be used to predict future fault configurations.

Introduction

How do faults grow and evolve? Why do some faults become abandoned and others develop? This question has typically been addressed using the well-established Mohr-Coulomb criterion for fault development. This criterion is based on empirical data from laboratory rock failure experiments and has been successfully used to predict fault

growth. Because the Mohr-Coulomb failure criterion is empirical and not based on a theory of physics, we are uncertain how to apply the criterion to conditions outside of the lab. For example, the viability of scaling laboratory experiments on small samples up to the kilometer scale is uncertain. If we can use a fault growth criterion based on principles of physics, we would be able to predict fault evolution at a variety of spatial and temporal scales. The San Gorgonio Knot is a portion of the San Andreas fault in southern California with a complex but distinct record of changing fault geometry. In the past one million years alone, the active strand of the San Andreas fault through the restraining bend of the San Bernardino Mountains has changed configuration at least twice. The most recent of these changes may help us to understand how fault systems evolve.

My goal with this work is to gain a better understanding of the fault evolution of the San Gorgonio knot using Boundary Element Method numerical modeling. I propose that fault systems tend to evolve to become more mechanically efficient, decreasing the work required to accommodate strain (e.g. Cooke and Murphy, 2004; Del Castello and Cooke, 2007; Olsen et al., 2008). Mechanical efficiency increases when fault surfaces grind away asperities, become smooth and the fault surfaces slip more easily. If the fault geometry changes or the tectonic stress field changes, faults may decrease in efficiency. In such situations, new faults may propagate to accommodate the elastic strain energy stored around the older, inefficient faults (e.g. Griffith and Cooke, 2004; Olsen et al., 2008). To evaluate the mechanical efficiency of the modeled fault system in the San Bernardino Mountains over the last 500 Ka, I investigate the change in net-slip, uplift and strain energy density pattern between simulations at different evolutionary stages. A benefit of this study is the insight provided to seismic hazard assessment in southern California. The

San Gorgonio Pass region is overdue for a large earthquake (Weldon et al., 2005). A large earthquake on this portion of the San Andreas fault could be catastrophic to the populated Los Angeles and San Bernardino areas as well as many other surrounding regions (e.g. Olsen et al., 2008). Understanding how this complex fault system evolves may aid in the forecasting of earthquakes. This type of study may also shed light on the mechanism of formation and evolution of restraining bends in other areas such as the Dead Sea fault zone (e.g. Gomez et al., 2007).

In this study, I will evaluate the mechanical efficiency of the San Gorgonio Pass region of the San Andreas fault at various stages in the past 500 Ka. Each modeled evolutionary stage is created using the southern California Earthquake Center's Community Fault Model (CFM; Plesch, 2007). Using this three-dimensional composite of all active and formerly active fault surfaces in southern California, in conjunction with the geologic evolution model of Matti and Morton (1993) I create three-dimensional fault models of the three different fault configurations that have been active within the San Gorgonio knot over the past 500 ka.

Geologic Background

Uplift of the San Bernardino Mountains

The San Bernardino Mountains have been uplifting for the last few million years (Spotila et al., 1998). The mountain range is composed of roughly east-west trending, fault bounded blocks that are larger in the northern portion of the range and decrease in both size and width closer to the San Andreas fault, which bounds the range to the south (Spotila et al., 1998). Allen (1957), Nicholson (1996), Spotila et al., (1998), Matti et al.,

(1992), and Yule and Sieh (2003) propose that two opposing thrust faults worked together to form the San Bernardino pop-up structure; the North Frontal thrust and the dipping San Andreas fault. The larger northern blocks of San Bernardino Mountains are uplifted by the North Frontal thrust zone (Figure 3.1; Meisling, 1984; Spotila et al., 1998), which has been active to varying degrees for at least the past 500 ka. Between 500 Kya and 125 Kya, greatly reduced dip-slip on the North Frontal thrust slowed uplift rates of the northern San Bernardino Mountain (Meisling, 1984). (U-Th)/He thermochronology indicates 3-6 km of uplift in the Yucaipa Ridge in the past 1.8 Ma (Spotila et al., 2001), though this uplift may have either all occurred prior to 1 Mya at a rate of ~5-7 mm/year or the Yucaipa Ridge may still be uplifting today at much slower rate (Spotila et al., 2001). Geologic evidence also suggests that the uplift in the Yucaipa Ridge occurred within the last 1.5 Mya (Yule and Sieh, 2003), and steep, rugged topography indicates that uplift is still occurring today in the southern most blocks of the San Bernardino Mountains (e.g. Matti et al., 1992). Spotila et al., (1998) suggest that the uplift localized north of the Mission Creek strand of the San Andreas in the location of the Yucaipa Ridge block did not occur at the same rate or in the same time period as the uplift of the Morongo block located north of the San Gorgonio thrust (Figure 3.1). The Morongo block, another of the southern San Bernardino blocks, has experienced only 2 km uplift in the last 2 million years (Spotila et al., 2001).

Present Day Fault Geometry and Slip Rates

The North American/Pacific plate motion is partitioned, for the most part between the San Andreas and San Jacinto fault systems. The Eastern California Shear Zone and other secondary faults also accommodate a portion of the overall plate motion. The San

Andreas fault from the northwest to southeast through the San Gorgonio Knot is comprised of the vertical Mojave segment of the San Andreas, which slips at 24.5 ± 3.5 mm/yr (Weldon and Sieh, 1985) near Cajon Pass where the fault transitions in the sub-vertical San Bernardino strand of the San Andreas fault (Figure 3.1). The San Bernardino strand of the San Andreas fault is the western boundary of a 20-km-wide restraining bend step over (Figure 3.1). The San Bernardino strand has been active for the last 125,000 years and has experienced 3 km of horizontal offset (Matti et al., 1985) giving a time averaged slip rate of 24 mm/yr. Estimates of recent slip rate along the San Bernardino strand of the San Andreas fault range between 2.6 and 17 mm/yr (Orozco, 2004; McGill et al., 2006; McGill et al., 2007) with slower slip rates to the south. Though the San Bernardino strand of the San Andreas fault and the San Gorgonio thrust are connected at depth, at the surface the San Bernardino strand turns south-west the near San Gorgonio Canyon and is only indirectly connected with the San Gorgonio thrust via the southern most tip of the Grady Ranch fault (Figure 3.1; Yule and Sieh, 2003).

The San Gorgonio thrust bounds the restraining bend step-over to the south (Figure 3.1; Yule and Sieh, 2003). The thrust has a saw-tooth-like geometry (Matti et al., 1985; Matti and Morton, 1993; Yule and Sieh, 2003). The northwest trending segments are oriented parallel to the overall plate motion and accommodate right lateral strike-slip, while the northeast trending segments exhibit reverse slip. The San Gorgonio thrust formed to accommodate contraction and uplift associated with the restraining bend in the San Bernardino Mountain segment of the San Andreas fault (Morton and Matti, 1993). The thrust fault has a strike-slip rate of 5.8 ± 0.8 mm/yr (Yule et al., 2001) and a reverse-

slip rate of 1.0-1.3 mm/yr (Matti et al., 1992). The eastern tip of the San Gorgonio thrust connects to the Garnet Hill and Banning strands of the San Andreas fault.

The south dipping North Frontal thrust is another active thrust fault in the region but is not part of the San Andreas fault. The North Frontal thrust is located to the north of the San Gorgonio thrust and has a dip-slip rate of >0.5 mm/yr for the last 2-3 Ma (Spotila and Sieh, 2000).

The parallel Garnet Hill fault and the Banning strand of the San Andreas fault are interpreted to merge into one north-dipping fault surface at a depth of 5 km (Figure 3.1; Yule and Sieh, 2003). Both faults have recent strike-slip rates of less than 1 mm/yr (Langenheim et al., 2005) though the Banning is a older strand of the San Andreas which became reactivated with the new Garnet Hill fault in the present day geometry (Matti and Morton, 1993). Where the Garnet Hill fault/Banning strand of the San Andreas fault connect with the San Gorgonio thrust the structure dips to the north. The Garnet Hill fault/Banning strand of the San Andreas becomes increasingly steep to the southwest and is nearly vertical where the fault merges into the Coachella Valley segment of the San Andreas fault to the south-west.

The Coachella Valley segment of the San Andreas fault is a relatively straight, sub-vertical fault that runs along the eastern shore of the Salton Sea (Figure 3.1; Matti and Morton, 1993). South of the Indio Hills, where the strike-slip rate on the fault is 9 - 15 mm/yr (Behr et al., 2007), the fault bifurcates. The south-western fork transitions into the active Garnet Hill/Banning fault zone (Yule and Sieh, 2003). The presently active north-eastern fork, from which the 9-15 mm/yr slip rates is determined, has offset Holocene alluvium (Matti and Morton, 1993; Behr et al., 2007), though at the northern tip

of the eastern fork, the fault turns west and becomes inactive (Figure 3.1; Matti et al., 1985). At this location the eastern fork bifurcates again into two formally active main strands of the San Andreas fault; the Mission Creek strand and the Mill Creek strand.

In the San Gorgonio pass region, the San Jacinto fault is a sub vertical fault that runs parallel to the San Andreas fault. The San Jacinto fault formed around 1.5 Mya and is a series of en echelon faults with no concrete evidence of connection with the San Andreas fault at the fault's northern tip (Morton and Matti, 1993).

Eastern California Shear Zone

The Eastern California Shear Zone (ECSZ) is a series of north-south and east-west trending faults located to the north of the San Gorgonio knot that accommodate around 15% of the Pacific/North American right-lateral plate motion (Figure 3.1; Sieh et al., 1993). The combined slip rate of the ECSZ is $\leq 6.2 \pm 1.9$ mm/yr (Oskin et al., 2008). The faults of the ECSZ were not originally formed in order to accommodate strike-slip motion as they do now, but instead were formed as normal faults during Miocene extension in the Basin and Range province (e.g. Oskin et al., 2008). Recent strike-slip earthquakes that have occurred along the faults of the ECSZ include the Landers earthquake (M_w 7.3) of 1992 and the Hector Mine earthquake (M_w 7.1) of 1999. The proximity of the ECSZ to the San Andreas and San Jacinto faults and the shared plate motion between the fault zones suggest that the ECSZ may play a role in the evolution of the San Andreas fault.

The Mojave Desert portion of the ECSZ is separated from the northern portion of the ECSZ by the Garlock fault. The Garlock fault is a left-lateral strike-slip fault that has been active for at least the last 2.2 Ma with a slip rate of 0.7 – 9 mm/yr (Clarke et al.,

1984; McGill and Sieh, 1991; McGill and Sieh, 1993) and intersects the San Andreas fault at the Big Bend (e.g. McGill and Sieh, 1991). The Mojave Desert portion of the ECSZ has been actively accommodating right-lateral plate boundary shear for approximately 10 – 6 Ma (Dokka and Tavis, 1990; Oskin and Iriondo, 2004).

Chronology of the San Andreas Fault Active Fault Geometry: Past 1 Ma

The Mission Creek strand of the San Andreas fault was the dominant strand of the San Andreas fault in the San Gorgonio Pass region during the majority of the Pliocene and accommodated 89 km of right lateral slip. This yields a time averaged strike-slip rate of 24.5 mm/yr. In the early Quaternary, two major complexities were introduced that changed the dynamics of the system; the San Jacinto fault and the San Gorgonio thrust (Figure 3.1). After around 2.5 Mya the Mission Creek fault, which was straight at this point, begins to bend to the west and by 1.2 Mya strike-slip had substantially slowed in the area of the San Gorgonio knot and the Mission Creek fault has a 60-70 □ north-dip (Matti and Morton, 1993, Langenheim et al., 2005). Decreased strike-slip along the now curved Mission Creek strand of the San Andreas was followed by the fault's abandonment around 500 Kya and the birth of the straighter Mill Creek strand of the San Andreas fault (Matti and Morton, 1993; Matti et al., 1985, Langenheim et a., 2005). The trace of the vertical Mill Creek strand of the San Andreas extends 60 km from the bend in the Mission Creek fault to the San Bernardino strand of the San Andreas fault (Figure 3.1). The Mill Creek strand slipped 8 km over 375 Ky with a time averaged slip rate of 22.4 mm/yr, before the Mill Creek strand was abandoned around 125 Kya for the present day San Bernardino and Garnet Hill strands of the San Andreas fault (Matti and Morton, 1993; Langenheim et al., 2005).

Numerical Investigations

The numerical investigations of this study have two goals. First, I test that my models adequately simulate present day deformation, for which I have the most geologic data. Once confident the models can simulate deformation of the southern San Andreas, I evaluate the transitions in fault geometry of San Andreas fault during the last 500 Ky of evolution. Starting with the abandonment of the Mission creek strand, I investigate the evolution of the fault system's mechanical efficiency.

I use Poly3D, a Boundary Element Method (BEM) modeling code to simulate deformation along the faults of the San Gorgonio knot. The triangular elements of Poly3D can replicate the three-dimensional geometry of intersecting irregular fault surfaces more precisely then rectangular elements. BEM only requires the discretization of fault surfaces while the Finite Element Method requires discretization of the whole volume. Minimizing discretization decreases model building and run time as well as discretization error (Crouch and Starfield, 1990). Poly3D has been successfully used to model crustal deformation associated with complex fault systems (e.g.Pollard et al., 2002; Muller and Aydin, 2003; Griffith and Cooke 2004; Griffith and Cooke, 2005; Olson and Cooke, 2005; Cooke and Marshall, 2006; Marshall et al., 2008).

For the material properties of this model, I prescribe a Poisson's Ratio of 0.25 and a Young's Modulus of 30 GPa to the model half space. These parameters represent an average of the different rocks types in the San Gorgonio Pass region. I insert a broad, horizontal detachment at a depth of 35 km to serve as the base of crust (Figure 3.2). This depth is chosen to match the imaged depth of the Mohorovičić discontinuity in this region (Magistrale et al., 2000). The horizontal detachment is allowed to slip freely, simulating,

to the first order, the distributed deformation expected below ~25 km in this region. The fault surfaces from the CFM are extended through the crust to the horizontal detachment. To simulate the regional deformation, I prescribe an overall N52˚W, 45 mm/yr right-lateral displacement onto the outer edges of the detachment to mimic plate motion (e.g. Bennett et al., 1999). The edges of the detachment are far from the San Gorgonio Pass study area in each direction to minimize edge effects (>300 km). If faults extend to the edge of the model, the distal tips are also assigned a strike-slip rate (Figure 3.2). This prescribed strike-slip along the fault tips is used to simulate infinitely long faults within this finite model. All faults and the detachment are prescribed zero opening in the normal direction to insure the faults do not open or interpenetrate and are shear-traction free, allowing the faults to slip freely in response to the prescribed displacement and interact with each other. By dictating that the faults be weak in shear throughout the brittle crust, my geologic models simulate the cumulative interseismic and coseismic deformation within the time modeled. The simulated time for each model is arbitrarily 1000 years; Because the models are elastic, the same geologic slip rate will result from any modeled length of time. The results of three-dimensional models of active faulting above a deep seated horizontal detachment match well the geologic deformation in southern California (Cooke and Marshall, 2006; Marshall et al., 2008; Meigs et al, 2008).

Present Day Model Validation

Dair and Cooke (in press) show that a three-dimensional model that contains only the present day San Andreas and San Jacinto faults matches well the geologic slip rates along the San Andreas fault. In this study, I have added a number of active secondary faults including the Mojave Desert section of the ECSZ. evolution models, I want to be

sure this new present day model also matches the geologic slip rate and uplift data for the region. Model strike-slip rates along several faults are compared with geologically observed and interpreted strike-slip rates (Figure 3.3). For segments of the San Andreas that have parallel strands, the strike slip along both stands is summed in Figure 3.3. Additionally, the strike-slip rate along the eastern branch of the northern fork of the Coachella Valley segment of the San Andreas fault, separate from the western fork, is shown for comparison to the geologic slip rate collected along that strand.

Variations in strike-slip rate due to addition of secondary faults occur at the southern tip of the San Bernardino strand, the San Gorgonio thrust, the Garnet Hill faultand the Coachella Valley Segment. The addition of secondary faults decreases strike-slip along the San Gorgonio thrust by ~ 5 mm/yr (Figure 3.3). The slower strike-slip along the San Gorgonio thrust falls below the range of the geologic slip rate (Yule et a., 2001), while the lower strike-slip along the San Bernardino strand of the San Andreas fault at Burro Flats (Orozco, 2004) fits the geologic slip rate better. The decrease in strike-slip along both the San Bernardino strand and the San Gorgonio thrust fault could be caused by the incomplete connection of the San Gorgonio thrust to the San Bernardino strand of the San Andreas fault. Previous models by Dair and Cooke (in press) considered these faults fully connected while here, the faults are only connected below 4.5 km. By disconnecting these two faults at the surface as the geology indicates, these models are able to more accurately simulate local uplift. When the San Bernardino strand and the San Gorgonio thrust are connect at the surface of the Earth in the model including secondary faults, the western portion of the San Gorgonio thrust acts as a normal fault instead of a thrust fault as mapped.

With the addition of secondary faults, the combined strike-slip from the parallel Garnet Hill fault and Banning strand of the San Andreas fault increases from west to east along the structure. At the western end of the Garnet Hill fault and Banning strand, the strike-slip rate is decreased by ~5 mm/yr with the addition of secondary faults, whereas on the eastern end of the structure, the strike-slip rate is similar to the model of Dair and Cooke (in press). The decrease in net-slip along this structure may have to do with reduced slip rates along the San Bernardino strand and the San Gorgonio thrust. The large jump in strike-slip rate south of the Garnet Hill fault arises from the presence of the fork of the northern Coachella Valley segment of the San Andreas fault. The Garnet Hill fault is only directly connected to the western branch of the fork and not the eastern branch, which creates a sharp change in strike-slip rate. The strike-slip along the western branch of the northern Coachella strand of the San Andreas matches the lower end of the slip rate range determined by Behr et al 2007.

The modeled strike-slip rate distribution at the Earth's surface of the San Jacinto fault decreases with addition of secondary faults (Figure. 3); however, neither the model with only primary faults nor the model with secondary faults matches the available geologic slip rates (Figure 3.3). The mismatch of slip rates along the modeled San Jacinto fault may have to do with the over simplification of the highly echelon geometry of the San Jacinto fault in our models.

I also investigate surface distributions of strike-slip rate at the Earth's surface along a few of the secondary faults in the model (Figure 3.3). The modeled strike-slip rate distribution along the Garlock fault matches 4 of 7 geologic slip rate sites at the specific study locations, and nearly fits 5 of 7 sites (Figure 3.3). The modeled strike-slip

rate distribution of the Blackwater, Calico, and Hidalgo faults fit only one geologic slip rate range out of three, but comes close to a second (Figure 3.3). Along the Helendale South fault, the geologic model strike-slip distribution at the Earth's surface fits the one geologic strike-slip rate range.

The modeled dip-slip rates at the Earth's surface along the San Gorgonio thrust (0.08 -6.51 mm/yr reverse slip) overlaps with the geologic dip-slip rate (1.0-1.3 mm/yr; Matti at al., 1992). The model surface dip-slip along the North Frontal thrust (1.26-3.54 mm/yr) fits the geologic reverse slip rate of >0.5 mm/yr, though this geologic range is broad (Spotila and Sieh, 2000).

The modeled present day uplift rates also fit well within thermochronomeric uplift rates (Figure 3.4; Spotila et al., 2001). The modeled uplift from the Yucaipa Ridge fits within the 1-7 mm/yr range (Figure 3.4). The present day modeled Morongo block uplift also fits within thermochronometric uplift of ~1 mm/yr (Figure 3.4; Spotila et al., 2001). Temporal and spatial variations in uplift will be discussed further below.

Though the fit to geologic data is not exact within complex locations along the San Andreas fault and the other secondary faults, I believe the overall fit and trend in strike-slip rates and uplift pattern at the Earth's surface accurately capture the majority of the fault deformation and indicates that these models can be considered useful tools in the analysis of the fault system.

Assessment of Mechanical Efficiency

Working under the assumptions that fault systems evolve to become more mechanically efficient, I am able to investigate the evolution of the fault system over the past 1 Ma by analyzing the mechanical efficiency of each different active fault geometry

(Del Castello and Cooke, 2007). Cooke and Murphy (2004) show that the mechanical work budget of a fault system can be calculated as:

$$W_{system} = W_{gravity} + W_{internal} + W_{friction} + W_{seismic} + W_{propagation} \quad \text{(Eq.1)}$$

The total deformational work of a fault system, W_{system}, includes work against gravity, $W_{gravity}$, internal work of deformation, $W_{internal}$, work against frictional sliding, $W_{friction}$, released seismic energy, $W_{seismic}$, and fault initiation and propagation energy, $W_{propagation}$. Some of these work are stored in the system, (e.g. $W_{gravity}$ and $W_{internal}$) while others are lost to the system. $W_{seismic}$ produces seismic radiation energy that is lost to the system as ground shaking.

The most efficient fault system minimizes the total stored energy by transferring this work to $W_{seismic}$ via fault slip. With this work lost, such fault systems will require less total work to accommodate future deformation than an inefficient fault system that produce no earthquakes. Consequently, fault systems evolve to maximize $W_{seismic}$, which requires maximizing slip. By maximizing slip along the faults, the system expends less energy deforming the surrounding rock ($W_{internal}$), meaning that the system is more mechanically efficient. With increased uplift, the fault system does more work against gravity and is therefore less mechanically efficient. The three-dimensional numerical models used in this study do not incorporate propagation due to limitations of the modeling code. Instead of examining work explicitly I assess the mechanical efficiency of the models using uplift and slip as proxies for work against gravity and internal work.

Strain Energy Density Predicts Fracture Propagation

Strain Energy Density (SED) is the elastic strain energy that is stored within the host rock (Jeager and Cook, 1976). Areas of high SED in a host rock are areas of high

stress that experience inelastic deformation, such as micro cracks. Though my models do not allow fault propagation, SED can be used to predict areas of inelastic deformation and fault propagation (Du and Aydin, 1993; Okubo and Shultz, 2005; e.g. Cooke and Kameda, 2002; Olson and Cooke, 2005). Olson and Cooke (2005) show that the, strain energy density pattern of a fault system is more reliable than using either energy release rate or Navier-Coulomb stress for characterizing and predicting fault propagation path.

Evolution Model Set-Up

Using the chronology of the San Bernardino Mountains segment of the San Andreas fault and the CFM, I created three-dimensional models of three distinct fault configurations of San Andreas fault evolution (Matti and Morton, 1993; Langenheim el al., 2005). Each fault configuration contains the San Andreas from the Mojave Desert segment to the Coachella Valley segment as well as a simplified version of the San Jacinto fault (Figure 3.1; Figure 3.5). Each model configuration also contains the active secondary faults in the area of the San Gorgonio Pass (Figure 3.5) as well as the Mojave Desert section of the ECSZ. The difference between each of the three evolution models is the main strand of the San Andreas fault within the San Bernardino Mountain segment. The first model configuration is that of the San Andreas > 500 Kya when the kinked and north dipping Mission Creek strand was active (Figure 3.5 A and B). The second model represents between 500 and 125 Kya when the Mill Creek strand of the San Andreas was the main active strand (Figure 3.5 C). In the present day configuration, the Mill Creek strand of the San Andreas is abandoned for the San Bernardino strand, the Garnet Hill fault/Banning strand, and the eastern most portion of the San Gorgonio thrust (Figure 3.5D).

Modeled Average Net-slip

The average net-slip rate per km^2 of fault surface of the whole system provides an overall assessment of the efficiency of the fault system. The modeled average net-slip increases by 48.3 % from the Mission Creek configuration to the Mill Creek configuration (Figure 3.6). The average net-slip decreases by 3.1 % from the Mill Creek configuration to the present day configuration. The net average slip of the entire system suggests that the Mill Creek configuration has the greatest mechanical efficiency. The Mission creek and present day configurations have less net-slip along fault surfaces than the Mill Creek configuration and consequently produce more off fault deformation.

To elucidate the cause for the change in overall net-slip from one model configuration to the next, I analyze slip rates on secondary faults. For this analysis, I exclude faults that either accommodate less than 1 mm/yr of net-slip in any one model configuration or show less than 0.25 mm/yr change in net-slip between two or more fault configurations (Figure 3.7). For example, though the Garlock and Camp Rock faults both accommodate greater than 3 mm/yr of net-slip in each model, the slip rates on these faults do not change significantly from one model to the next and therefore do not reveal changes in overall net-slip rate. The net-slip of several faults, including faults of the Eastern California Shear Zone, Blue Cut, San Andreas fault and North Frontal thrust is sensitive to model configuration.

The modeled weighted average slip on the faults of the ECSZ increase from 1.09 mm/yr in the Mill Creek configuration to 1.16 mm/yr in the present day configuration. This suggests that geologic slip rates measured over 500 Kya would be slower than present-day rates. Oskin et al., (2008) indicate that geodetically inferred slip rates along

the ECSZ (12 ± 2 mm/yr) measured over the past 5-10 years are presently twice that of the accumulated slip rate of the shear zone since the Miocene (≤ 6.2 ± 1.9 mm/yr). Variations in slip partitioning related to changing San Andreas fault geometry could account for some of the discrepancy between time averaged geologic slip rates and geodetic slip rates.

The Blue Cut fault is highly sensitive to active fault configuration. The left-lateral Blue Cut fault has a greater slip in the Mill Creek configuration than in either the Mission Creek or present day configurations (Figure 3.7). The increased net slip along the San Andreas during the Mill Creek configuration may facilitate slip along the Blue Cut fault.

The North Frontal Thrust and East North Frontal Thrust experience the most dip-slip in the Mission creek configuration (Figure 3.7). The dip-slip on the North Frontal Thrust decreases during the time of the Mill Creek strand of the San Andreas fault and increases from the Mill Creek configuration to the present day configuration, but does not reach the same level of activity as the Mission Creek configuration. The north-dipping strands of the active San Andreas fault during the Mission Creek and present-day configurations may act in concert with the south- dipping North Frontal Thrust to facilitate uplift of the San Bernardino Mountains. Consequently, when the vertical Mill Creak strand is active, dip slip along the North Frontal thrust may decrease because the south-dipping fault is not so effective an accommodating local contraction as when paired with an active north-dipping fault. Analysis of the uplift pattern will shed additional insight into the shifting activity of these faults.

Modeled Uplift Pattern

The modeled uplift rate maps show a distinct change in vertical deformation between the Mission Creek configuration and the Mill Creek configuration (Figure 3.8). During the modeled active period for the Mission Creek strand of the San Andreas fault, a maximum uplift rate of 5 mm/yr occurs in the area of the Yucaipa Ridge block in the Southern San Bernardino Mountains (square in Figure 3.8). The area of the San Bernardino Basin experiences a maximum down-drop rate greater than 2 mm/yr during the Mission Creek model. The range between maximum uplift and down-drop rates decreases in the Mill Creek model to around -1 to 1 mm/yr (Figure 3.8). While the uplift rates of the modeled San Bernardino Mountains are spatially variable in the Mission Creek configuration, the variation of uplift is much less throughout the San Bernardino Mountains in the Mill Creek configuration. The reduction in uplift rates in the Mill Creek model may arise because the south-dipping North Frontal thrust is not able to act in concert with a north-dipping strand of the San Andreas fault to uplift the mountains. The vertical Mill Creek strand is not as effective at uplifting the range as the north-dipping San Gorgonio thrust but because the Mill Creek strand has greater slip net-slip, the San Gogonio thrust not active enough to uplift mountains.

Within the present day model, uplift rates in the northern San Bernardino Mountains increase from the Mill Creek model (Figure 3.8). Two specific areas in the southern SBMs show increased uplift in the present day configuration. The sliver of land between the Banning strand and the Garnet Hill fault uplifts because the two faults merge at depth in the region; the land between them is squeezed up like a watermelon seed. The second area of uplift is located just north of the eastern most portion of the San Gorgonio

thrust, which is part of the Morongo block (circle in Figure 3.8). The Morongo block does not uplift in these models until the present day configuration when both the San Gorgonio thrust and the north dipping Garnet Hill fault, which underlie the block, are active.

Uplift analysis

My models show temporal and spatial variations in mountain range uplift rates that are related to the changing fault geometry during the evolution of the San Andreas fault. These temporal/spatial variations in the modeled uplift results reproduce the slower overall geologic rate of exhumation of the Morongo block as compared to the Yucaipa block. While the north dipping Mission Creek strand of the SAF is active, the dipping geometry facilitates uplift in the Yucaipa Ridge block area. The area of the Morongo block does not uplift until activity starts on the Garnet Hill fault and the San Gorgonio thrust, which underlie this block. Slowed dip-slip on the North Frontal thrust during the time of the active Mill Creek strand indicates a lull in uplift during the Mill Creek model, as compared to the Mission Creek and present day configuration models, though uplift never stops completely.

In addition to calculating uplift rates at specific configurations modeled, we can time-average the uplift rates from each configuration for comparison with thremochoronometric uplift rates. The time averaged modeled uplift rate of the western portion of the Yucaipa Ridge block is 3.5 mm/yr for the last 1.8 Ma (Figure 3.8). This modeled slip rates fit with in the time-average geologic uplift rates of 1.7- 3.3 mm/year (Spotila et al., 2001), when the time bias towards the Mission Creek configuration is taken into account. The time averaged modeled uplift rate for the Morongo block is -0.2

mm/yr for the last 2 million years (Figure 3.8), which does not fit well within the . ~1 mm/yr geologic time averaged rate (Spotila et al., 2001). When looking at these numbers it is necessary to understand that the time averaged uplift rates from the models are highly sensitive to small changes in the Mission Creek configutation uplift rates do to the significantly longer amount of time that is allotted the Mission Creek deformation in this comparison with geologic time averages from Spotila et al., (2001). The Morongo block is down dropping in the Mission Creek model configuration by ~0.6 mm/yr. If no uplift or down drop were happening the modeled time averaged uplift rate would be positive and come much closer to matching that of Spotila et al., (2001).

Using uplift as a proxy for work against gravity I can say that the decrease in work against gravity from the Mission Creek model, with an average uplift of 0.39 mm/yr, to the Mill Creek model, with an average uplift of 0.36 mm/yr indicates an increase in mechanical efficiency of the system. An increase in uplift between the Mill Creek and present day (0.37 mm/yr average uplift) geometries indicates a decrease in the mechanical efficiency of the system. The areas with high uplift rate, in the Mission Creek and present day configurations correspond with proximity to two dipping faults indicating, again, that the geometry of the fault surfaces in the San Gorgonio Pass controls the uplift pattern. In both the Mission Creek and present day configurations, less net-slip occurs along the San Andreas fault and slip is instead transferred to secondary structures including dip-slip on the North Frontal thrust.

Strain Energy Density

Areas of high SED are produced at the Earth's surface in each of the modeled fault configurations (Figure 3.9). The areas of high SED may indicate locations of new

fault development. Within the model high SED can be locally associated with element nodes so I focus my anylysis on areas of broad high SED. A broad area of high SED is associated with the northern tip of the San Jacinto fault in all model configurations. In the Mission creek configuration, high SED is also associated with the kink in the San Andreas fault (labeled 1 in Figure 9A) as well as between the North Frontal thrust and the San Andreas fault (labeled 2 in Figure 9A). Within the Mill Creek configuration, areas of high SED occur between the Mill Creek strand of the SAF and the San Gorgonio thrust (labeled 3 in Figure 9A) as well as between the eastern tip of the San Gorgonio thrust and the tip of the Western fork of the Coachella Valley segment of the SAF (labeled 4 in Figure 9B). The Mill Creek model does not have high SED between the North Frontal thrust and the San Andreas fault as did the Mission Creek model. In the present day configuration, high SED occurs between the active San Gorgonio thrust and Garnet Hill fault and the inactive Mill Creek fault (Figure 9C). The high SED within the San Bernardino Basin forms a solid band along the San Bernardino strand of the San Andreas fault and merges with the high SED north of the San Gorgonio thrust. High SED also occurs south of the North Frontal thrust in the present day model but not to the extent of that in the Mission Creek model (Figure 3.9).

Strain Energy Density Analysis

The SED associated with the kink in the Mission Creek configuration highlights the region of the Mill Creek strand formation (1 on Figure 3.9). The Mill Creek strand propagated though the high SED produced by the Mission Creek configuration and reduced the SED high in the area of the former fault kink as well as the SED high south of the North Frontal thrust (2 on Figure 3.9).

The propagation of the San Bernardino strand of the San Andreas in the present day model occurs within the high SED area north of the San Gorgonio thrust in the Mill Creek configuration (3 on Figure 3.9). Similarly, the Garnet Hill fault develops within the area of high SED at the tip of the western branch of the Coachella Valley segment of the San Andreas fault along the inactive, preexisting Banning strand of the San Andreas fault (4 on Figure 3.9).

Though the propagation of these two new faults suggest that areas of high SED facilitate fault propagation, the SED in the present day configuration is much greater then the SED in the Mill Creek configuration. Higher average SED in the present day model (9.5E-5 MPa) as compared to the Mill Creek model (7.7E-5 MPa) may be due to the preexisting San Gorgonio thrust that connects the San Bernardino strand and the Garnet Hill fault. Complexity is added to the system when the San Bernardino strand of the San Andreas fault and the Garnet Hill fault intersect the preexisting San Gorgonio thrust. This complexity increases the average SED in the present day model. Had the San Gorgonio thrust not existed already the San Bernardino strand/Garnet Hill fault connection may have been smoother causing the SED in the present day model to be less than that of the Mill Creek model.

Discussion and Implications

Bennett et al., (2004) suggest that the range in the geology slip rate data implies a switch in the partitioning of plate motion between the San Andreas fault and the San Jacinto fault in the last 1000 Ky, where the San Jacinto fault slips at a higher rate than the San Andreas fault before 125 Kya. Although Bennett et al., (2004) do not consider that slip rates may vary along the faults, a factor that could muddy their interpretation of the

geologic data, the idea of temporal trade-offs between fault systems has captured much interest in the community. Though our models have higher strike slip along the San Andreas than along the San Jacinto fault, strike-slip rates along the San Jacinto fault increase when and where strike-slip rates decrease on the San Andreas fault. In the more geometrically complex models (i.e. Mission Creek and present day), strike-slip increases on the San Jacinto fault and strike-slip decreases on the San Andreas fault compared to the Mill Creek model. Because my boundary conditions apply 10 mm/yr and 25 mm/yr to the south edges of the San Jacinto fault and San Andreas fault respectively in all models, any changes in slip are due to change in fault geometry and not tectonic boundary conditions. These boundary conditions, which simulate the present day fault system, may also prevent my models from having greater slip on the San Jacinto than the San Andreas fault as suggested by Bennett et al., (2004). Changes in the tectonic boundary conditions for the Mission and Mill Creek configurations could alter the slip partitioning along the San Andreas and San Jacinto faults, but such changes are not represented in these models.

The increase in net-slip and the decrease in uplift from the Mission Creek configuration to the Mill Creek configuration suggests that from 500 Kya to 125 Kya the San Andreas fault evolved to increase mechanical efficiency. The decrease in mechanical efficiency from Mill Creek to present day may indicate either that the model neglects some aspect of that deformation or that the fault system does not evolve to become more efficient.

Missing Aspect

While this study suggests that the San Andreas fault has evolved to become less mechanically efficient from the Mill Creek to the present day configuration, these models do not include frictional resistance along the fault surfaces, which could alter slip distribution and the work budget. The trend of the Mill Creek strand of the San Andreas fault changes along strike and the northern portion of the fault strand trends obliquely to the regional plate motion (Figure 3.10). The San Bernardino strand and the Garnet Hill fault within the present day configuration may be more favorably oriented for strike-slip because they deviate only 12-15˚ from the plate motion rather than 23˚ for the northern Mill Creek strand. With the inclusion of frictional resistance in the model, the present day configuration may be more mechanically efficient than the Mill Creek configuration if the northern Mill Creek experiences a large amount of frictional resistance. In models of fault development in accretionary wedges, Del Castello and Cooke (2007) show that new fore thrusts are more efficient than continued roof thrusting even though the fore thrusts produce greater internal work; the work savings of lesser frictional heating compensates for the increase in internal work. For the San Andreas fault, less frictional heating along more favorably oriented fault in the present day model may compensate for the greater internal work accumulated (as evidenced by greater SED in Figure 3.9) compared to the **Mill Creek model.**

Preliminary frictional models of the San Andreas and San Jacinto faults in the San Gorgonio Pass region have been run with a frictional coefficient of 0.4 to determine how the addition of friction would affect the net-slip within the Mill Creek configuration fault system as compared to the present day configuration fault system. These results are

preliminary due to a change in modeling code for the sake including friction to the models. The results from the new code, Poly3D-v2.1.8 do not match the results from the original modeling code used, Poly3D-v2.1. I am therefore, only discussing the possible implications of the results to follow.

The Mill Creek configuration models show a 22% decrease in net-slip with the addition of friction while the present day configuration model slip decreases 18% with the addition of friction (Table 1). The slip within Mill Creek configuration is more sensitive to the addition of friction than the present day model. When a frictional coefficient of 0.4 is added to the models, the Mill Creek model still has higher net slip than the present day model, however the difference is smaller. The percent reduction in slip rate difference from the Mill Creek model to the present day model is 23 % (Table 1). Though the Mill Creek configuration still slips faster then the present day configuration with the addition of friction, there is a substantial decrease in the percent difference in net-slip between the two model configurations. An increase in the frictional coefficient could facilitate the abandonment of the Mill Creek strand of the San Andreas for the present day fault geometry

Transitional State

Alternatively, the San Andreas fault may be working to become more efficient with the present day geometry acting as a transitional state on the way to a state of even higher mechanical efficiency than the Mill Creek geometry. Both the San Bernardino strand of the San Andreas fault and the Garnet Hill fault may have utilized two separate strike-slip sections of the San Gorgonio thrust as one fault strand developed to the north and the other south. If the preexisting San Gorgonio thrust not been present, the San

Bernardino strand of the SAF may have connected directly to the Garnet Hill fault (Figure 3.11).

The Mill Creek strand of the San Andreas fault evolved to remove the left step in the San Gorgonio pass by removing the kink in the Mission Creek strand (Figure 3.11). The Mill Creek strand may have accommodated the high strain energy stored around the kink in the Mission Creek strand while still leaving the large bend at the southern end of the Mill Creek strand of the San Andreas (Figure 3.9 and 3.11). Propagation of the San Bernardino strand of the SAF and the Garnet hill faults further straightens the San Andreas fault from the Coachella Valley segment to the Mojave Desert segment and form segments of that are more parallel to the present plate motion. The preexisting San Gorgonio thrust becomes more active in the present day configuration as the thrust becomes integrated into of the main strand of the San Andreas fault and also accommodates contraction occurring in the San Bernardino Mountain area.

Conclusion

Three-dimensional models accurately simulate deformation along faults of the region. The main strand of the San Andreas fault in the San Gorgonio knot has changed twice in the last 500 ka. Using three-dimensional numerical modeling to analyze mechanical efficiency I have discovered the final stage of fault evolution in this area does not evolve to minimize the total work of the fault system. Mechanic efficiency increases from the Mission Creek configuration to the Mill Creek configuration, but decreases from the Mill Creek configuration to the present day configuration, as indicated by changes in uplift and net-slip.

The 3.1 % decrease in the weighted average net-slip rate between the Mill Creek configuration and the present day configuration may be due to the absence of work against frictional sliding in the models. Preliminary frictional models of the San Gorgonio Pass region indicate that the obliquity of the northern Mill Creek relative to plate motion may resist sliding and favor the abandonment of that strand and the development of the present day fault geometry configuration.

The areas of high Strain Energy Density from the Mission Creek and Mill Creek fault configurations correspond to areas of new fault inception in subsequent models. High Strain Energy Density areas in the present day configuration model may forecast a new strand of the San Andreas through the San Gorgonio knot. The present day configuration may be a transitional stage of relative mechanical inefficiency before the next stage of increased mechanical efficiency in the evolution of the San Andreas fault.

Table 3.1. Percent change with the addition of friction for Mill Creek and Present Day Models. The bottom line percentage indicates the reduction in difference between the freely slipping Mill Creek and present day models to the frictionally slipping Mill Creek and present day models.

	Freely Slipping (mm/yr)	**Fictionally Slipping (mm/yr)**	**Reduction with addition of Friction (%)**
Mill Creek	0.73	0.57	22%
Present Day	0.11	0.09	18%
Mill -> Present Day (changes in slip)	0.62	0.48	23% (reduction in difference)

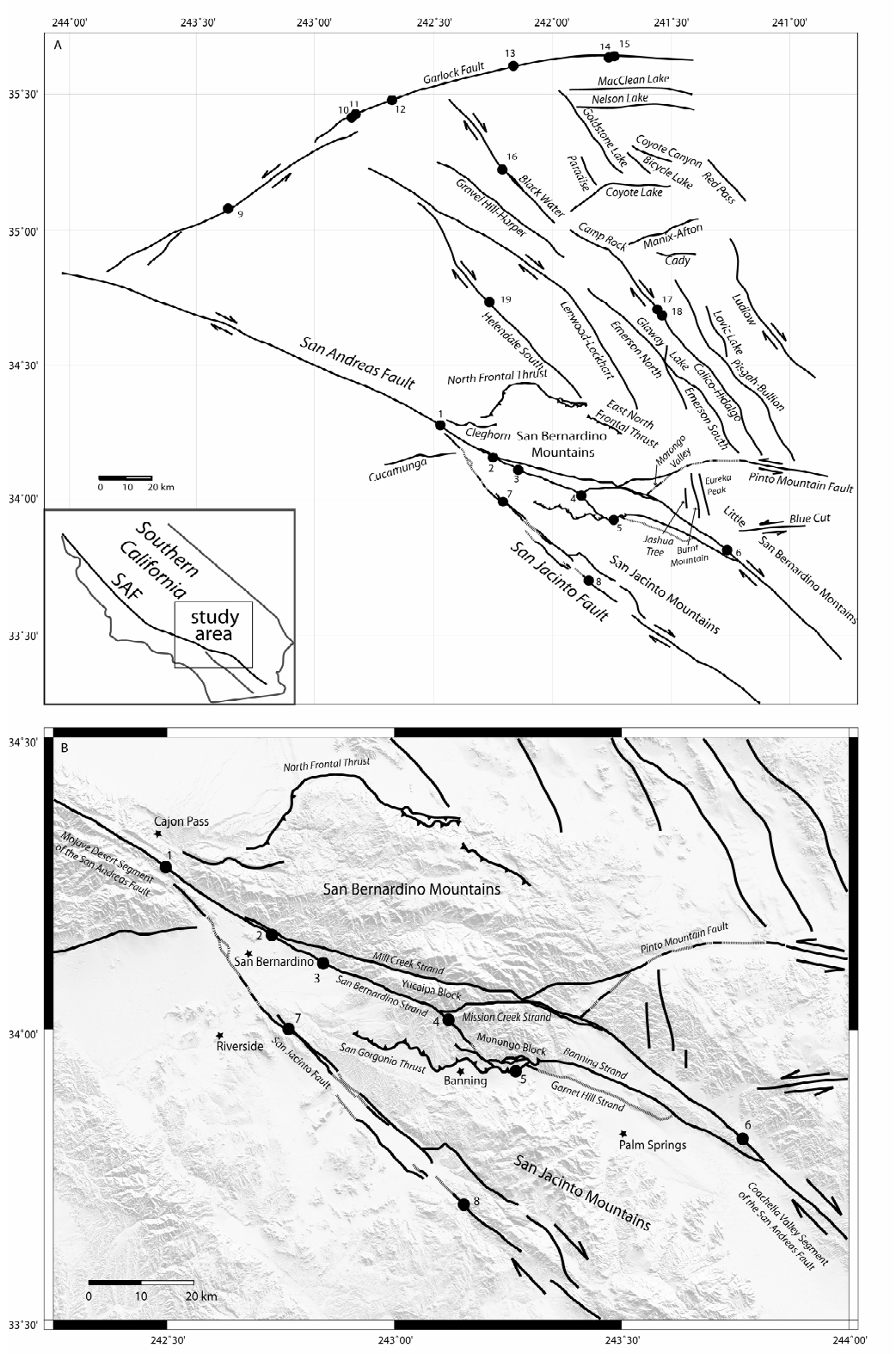

Figure 3.1. Area maps of the San Bernardino Mountain segment of the San Andreas fault in southern California.The dashed lines indicate faults with no surface trace. Black dots indicate locations of geologic slip rate studies used in model validation. Site 1, Cajon

Pass– Weldon and Sieh, 1985; site 2, Badger Canyon– McGill, 2007; site 3, Plunge Creek- McGill et al., 2006; site 4, Burro Flats – Orozco, 2004; site 5, Yule et al., 2001; site 6 - Behr et al., 2007; site 7 - Kendrick et al., 2002; site 8 - Rockwell et al., 1990 and Rockwell, 2006, site 9, 10 and 13– Clarke et al., 1984, site 11, 12 and 14 – McGill and Sieh, 1991, site 15- McGill and Sieh, 1993, site 16- Oskin and Iriondo, 2004, site 17- Oskin et al., 2007, site 18 and 19- Dokka 1983 and Dokka and Travis, 1990. A) contains all of the faults modeled in this study including the Eastern California Shear Zone, which includes all fault from Helendale South eastward. B) shows a close up of the San Bernardino Mountain area and the different fault strands that have been active in the last 500 Ky (modified from Matti et al. 1992).

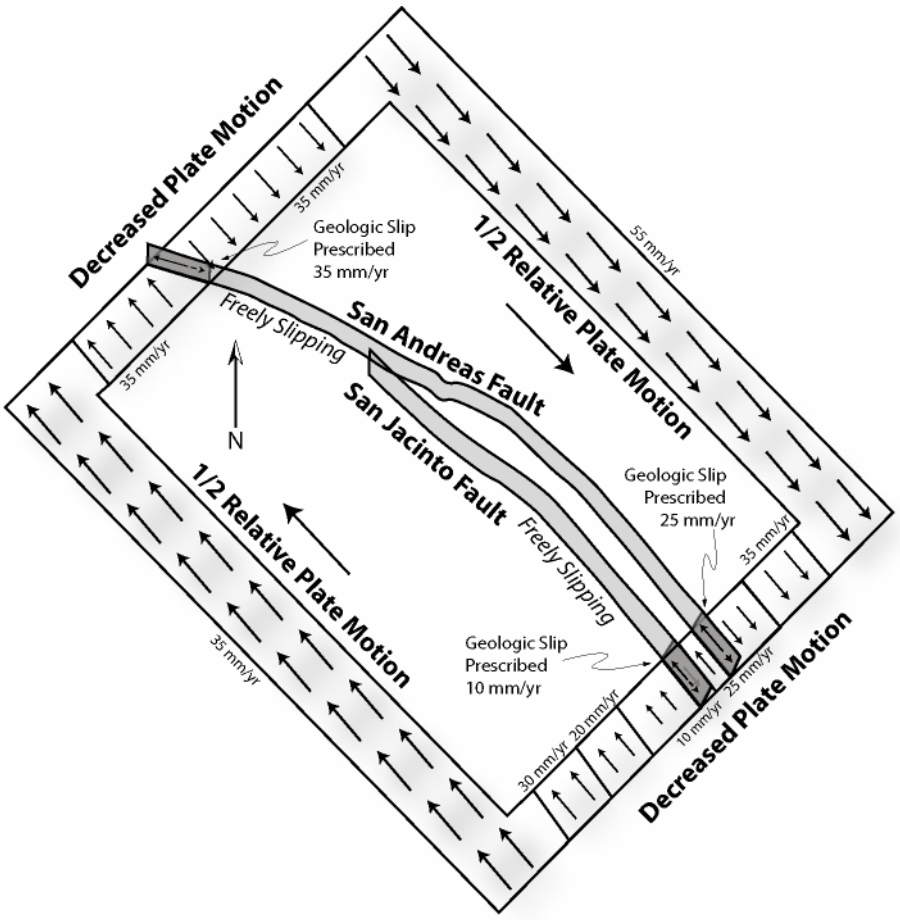

Figure 3.2. A schematic drawing of the loading of the models. The edges of the 35 km deep detachment as well as the distal tips of the primary faults have prescribed slip. The slip on the detachment is decreased incrementally as each section nears the strike-slip fault until slip on the section adjacent to the fault matches the prescribed slip on the fault tip. Most slip is prescribe on the eastern edge of the detachment than the western edge due to the plate bounding slip partitioned onto the Eastern California Shear Zone located to the north east of the San Bernardino Mountain segment of the San Andreas fault. In the center of the model, all faults slip and interact in response to the loading at the edges of the detachment.

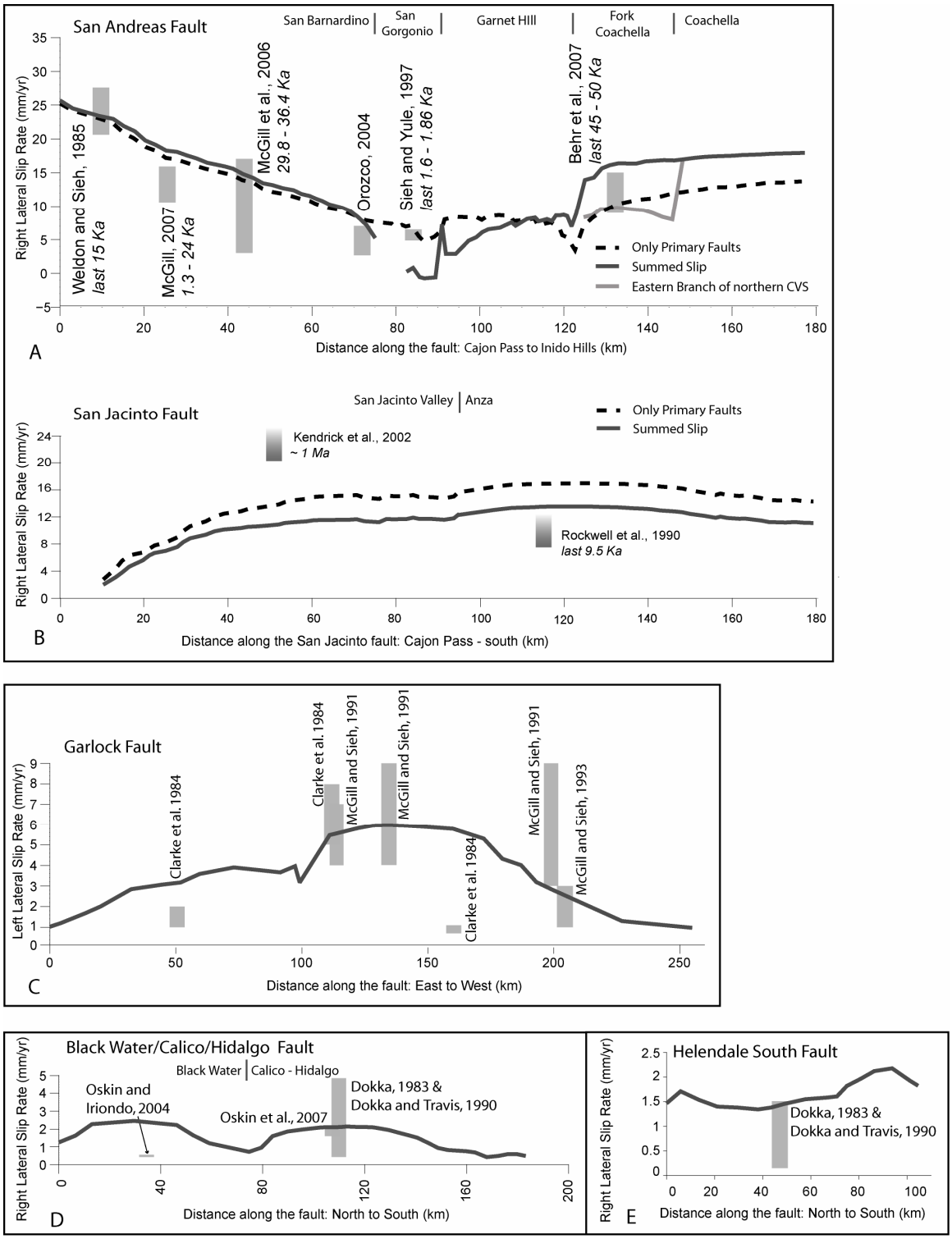

Figure 3.3. The modeled strike-slip distribution along the San Andreas fault (A), and San Jacinto fault (B) at the Earth's surface from the Cajon Pass to the Indio Hills. Gray boxes are geologic observed and interpreted strike-slip rate ranges at distinct sites along each fault. The San Andreas and the San Jacinto slip distributions from this study are in dark gray and are compared to the slip distributions from Dair and Cooke (in press) in dotted

black. The light gray section of slip distribution along the San Andreas fault is from the eastern branch of the northern fork of the Coachella Valley segment of the San Andreas fault alone as discussed in the text. The modeled surface strike-slip distribution along selected faults in the ECSZ that have geologic slip rates are also show (Figure 3.1); the Garlock fault (C), the Black Water and Calico-Hidalgo faults (D), and the Helendale South faults.

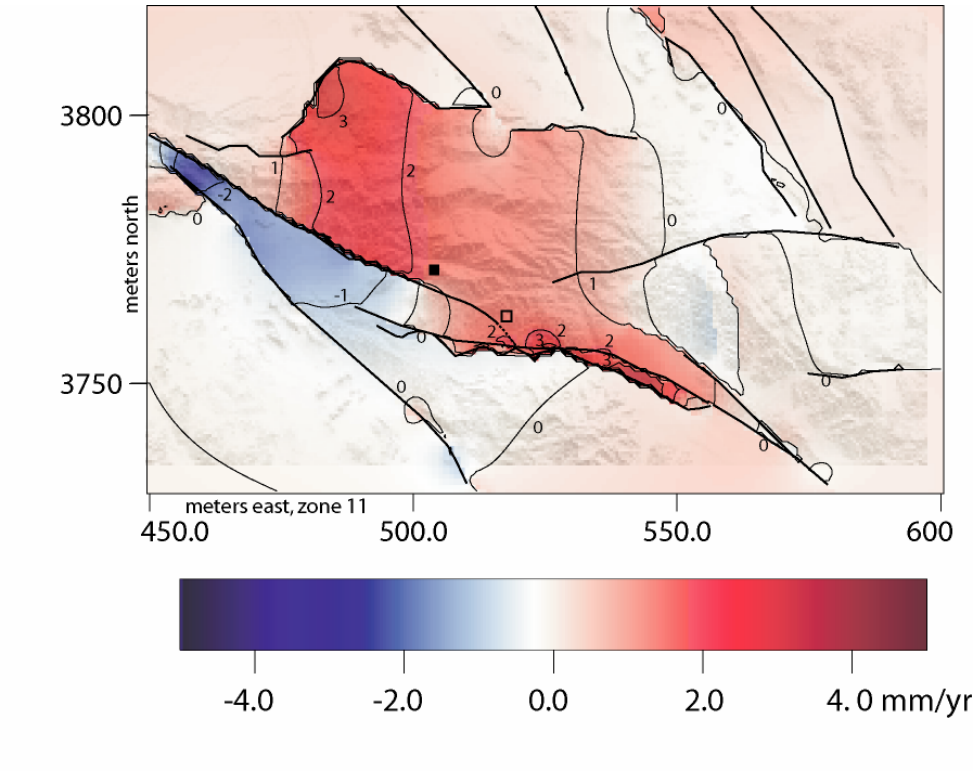

Figure 3.4. Geologic versus Modeled uplift rates. The open and closed squares the locations of thermochronometry done by Spotila et al., (2001) discussed in text. The closed square location has an uplift rate of 1-7 mm/yr (~1.4 – 1.7 Ma) in the Yucaipa Ridge block. The open square location has a time averaged uplift rate of ~1 mm/yr. Both modeled uplift rates match geologic uplift data.

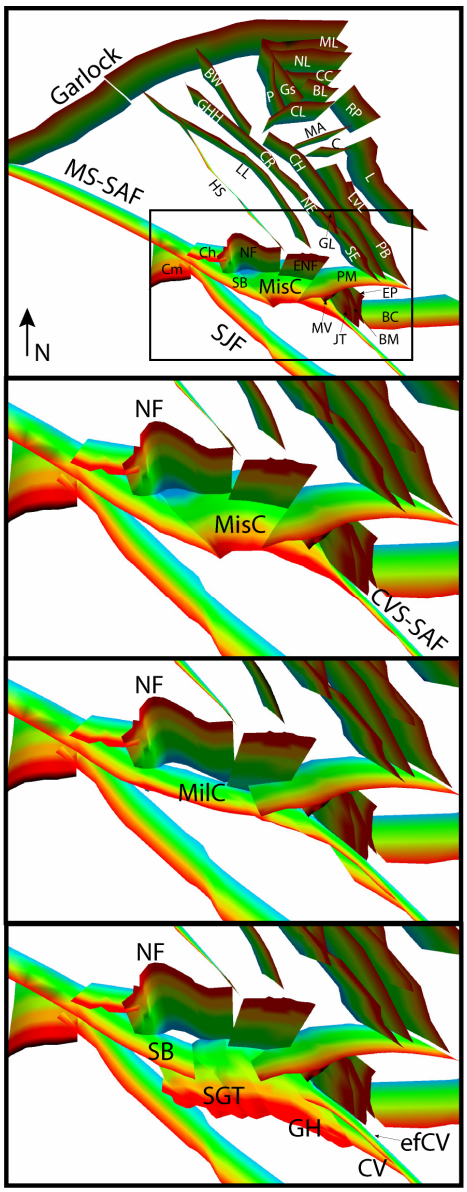

Figure 3.5. The fault configurations taken from the CFM and extended to 35 km depth. A) Shows the entire Mission Creek Configuration. The black box shows each configuration close up; B) Mission Creek Configuration, C) Mill Creek configuration and, D) present. The faults are color shaded to a depth of 35 km from red to blue. SJF = San Jacinto fault, MisC = Mission Creek Strand of SAF, MilC = Mill Creek strand of the SAF, SB = San Bernardino strand of the SAF, SG = San Gorgonio thrust, GH = Garnet Hill fault, HS = Helendale South, LL = Lenwood-Lockhart, GHH = Gravel Hill- Harper, BW = Black Water, CR = Camp Rock, NE = North Emerson, SE = South Emerson, GL = Galway Lake, P = Paradise, ML = MacClean Lake, NL = Nelson Lake, CC = Coyote Canyon, BL = Bicycle Lake, Gs = Goldstone, RP = Red Pass, MA = Manix-Afton, C = Cady, CL = Coyote Lake, CH = Calico-Hidalgo, LvL = Lavic Lake, PB = Pisgah-Bullion, L = Ludlow, PM = Pinto Mountain, MV = Morongo Valley, JT = Joshua Tree, EP = Eureka Peak, BM = Burnt Mountain, Cm = Cucamonga.

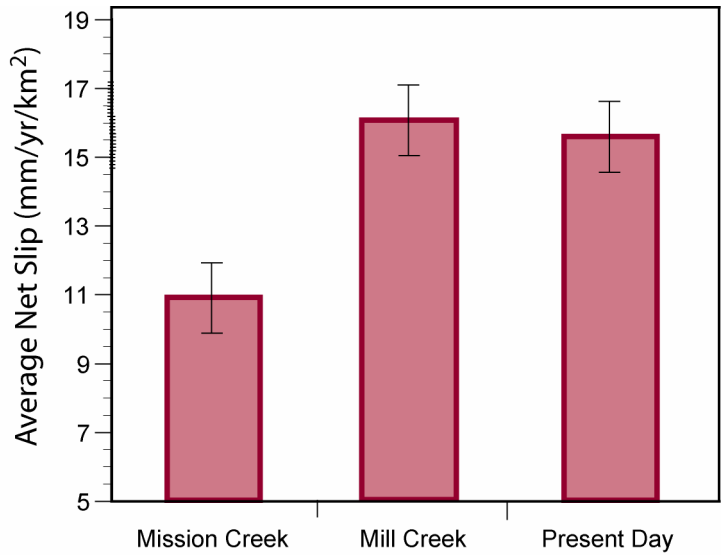

Figure 3.6. The weighted average net-slip. The weighted average slip of the entire system for each fault configuration is shown. The Mission creek has less slip than the Mill creek configuration indicating a increase in mechanical efficiency. The Mill creek configuration has more slip than the present day indicating a decrease in mechanical efficiency to present day. The error bars indicate the standard deviation.

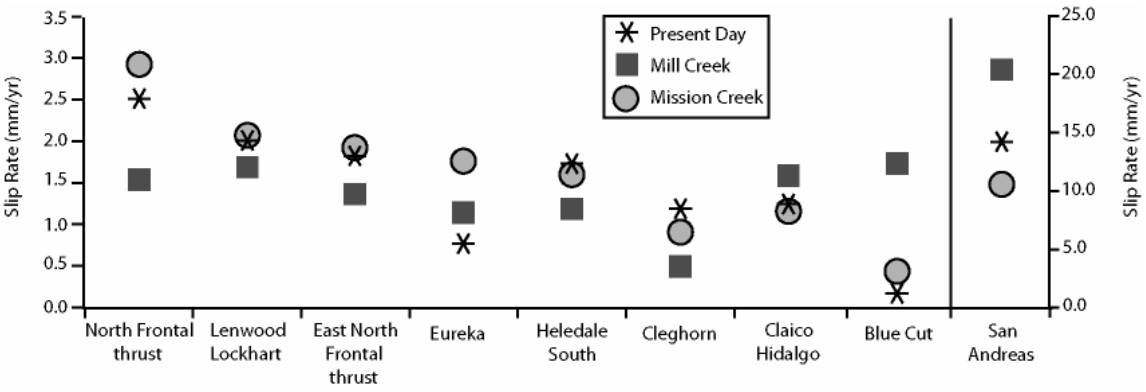

Figure 3.7. Net-slip rates on secondary faults. Faults with more than 1 mm/yr slip in one or more model configurations and that change slip more then 0.25 mm/yr between two or more model configuations are shown. The San andreas fault is shown for slip partitioning compairson. The North Frontal thrust and the left-lateral Blue Cut strike-slip fault show the greatest change between models. The Mission Creek and present day model seem to accomidate more contraction while the Mill Creek model accomidates extension.

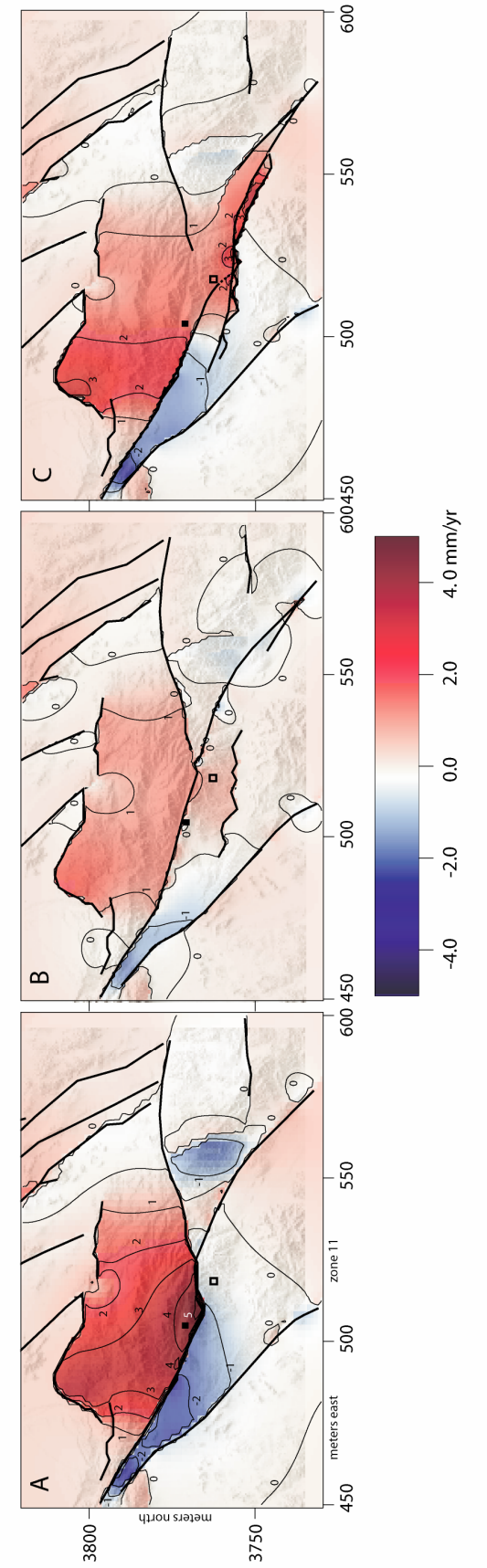

Figure 3.8. Vertical displacement maps. The A) Mission Creek, B) Mill Creek, and C) present day fault geometry configurations are overlain on a digital elevation map of the San Bernardino Mountains region. Uplift occurs at much higher rate in the Mission Creek configuration than the Mill Creek configuration. Uplift increases from the Mill Creek configuration to the present day configuration. The geometry of the fault greatly influences the uplift patterns. Closed and open squares represent thermochronometric uplift rate locations in the Yucaipa Ridge and Morongo blocks respectively. The modeled uplift rates demonstrate a spatially and temporally varying fit to the geologic data.

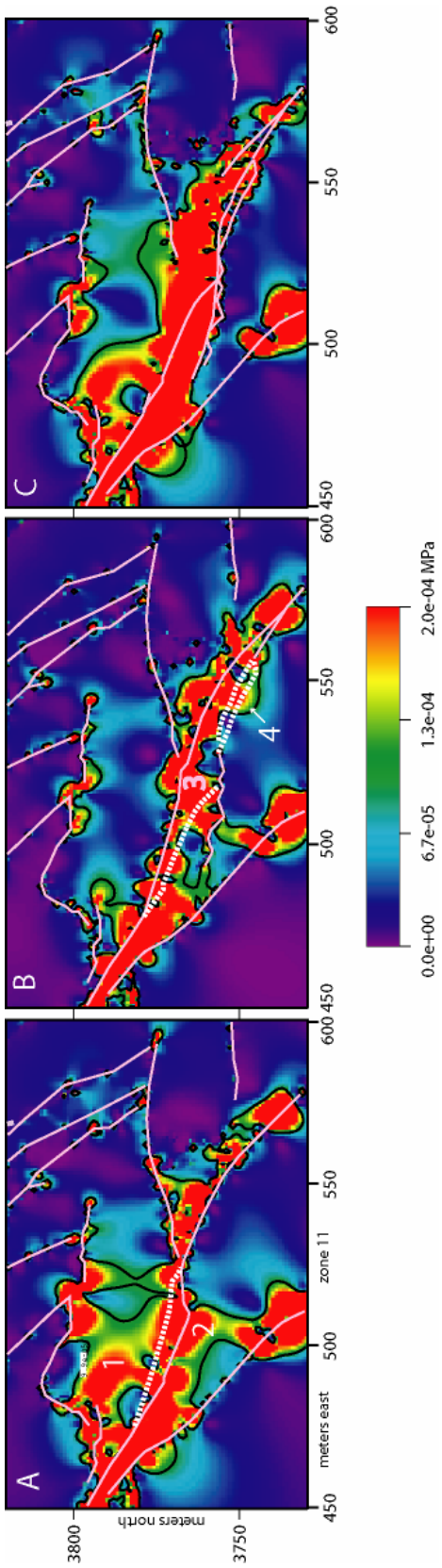

Figure 3.9. Strain energy density maps for each of the model configurations. Areas of high strain energy density are label are numbered the A) Mission creek model produced two regions of high SED (1 and 2) that disappear in the B) Mill Creek model, and may be associated with the propagation of the new Mill Creek fault. Incipient faults are shown in dotted lines. Similarly, region 4 in the Mill Creek configuration disappears with propagation of the Garnet Hill fault. The C) present day configuration has greater SED than the previous configurations. Each models produces an area of high SED between the north-most tip of the San Jacinto fault and the San Andreas fault. This might be relieved if the San Jacinto fault intersected the San Andreas fault.

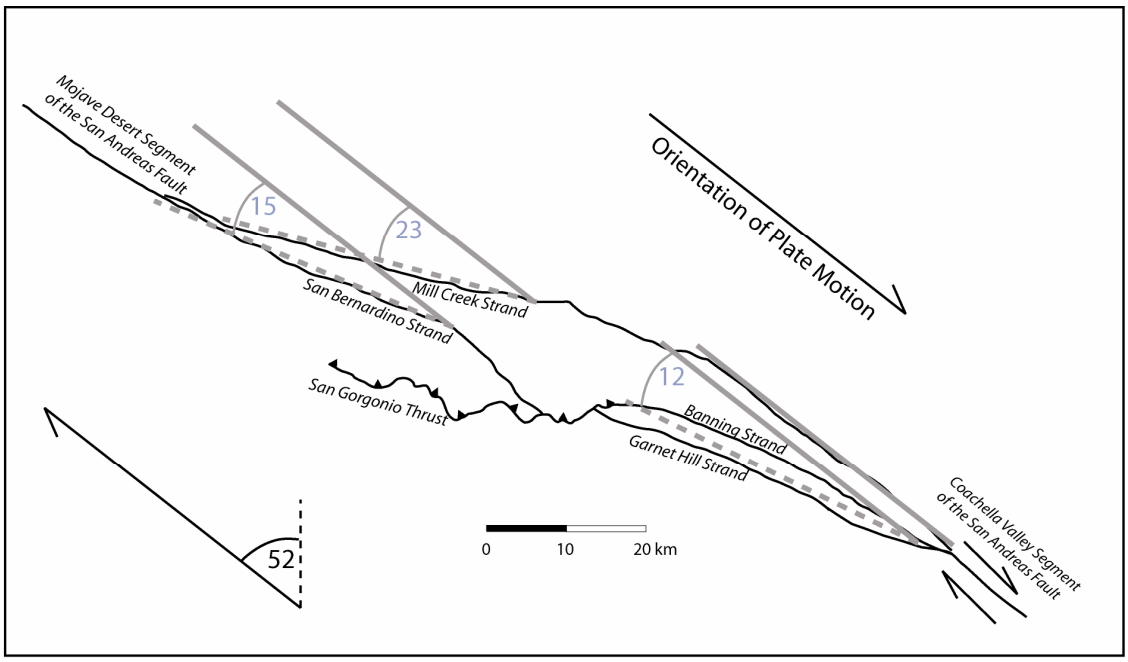

Figure 3.10. A comparison of the Mill Creek and present day configuration. The solid gray line is oriented at N52W, the regional plate motion in the area. The dotted gray lines show the trend of a given fault trace for comparison to the regional plate motion. The Mill Creek fault has two segments, one is almost exactly parallel with the regional plate motion and is still active today as the eastern fork of the northern Coachella Valley segment of the San Andreas fault. The northeast part of the Mill Creek fault trends 23 degrees from the regional plate motion. The San Bernardino segment of the San Andreas fault 15 degrees from the regional plate motion. The Garnet Hill/Banning strand of the San Andreas fault trends 12 degrees form the regional plate motion. Both of the present day San Andreas fault strands are at a smaller angle to the regional plate motion. This suggests that frictional resistance may be lesser on the San Bernardino strand and the Garnet Hill/Banning strand than on the Mill Creek strand of the San Andreas fault and may account for the abandonment of the Mill Creek strand.

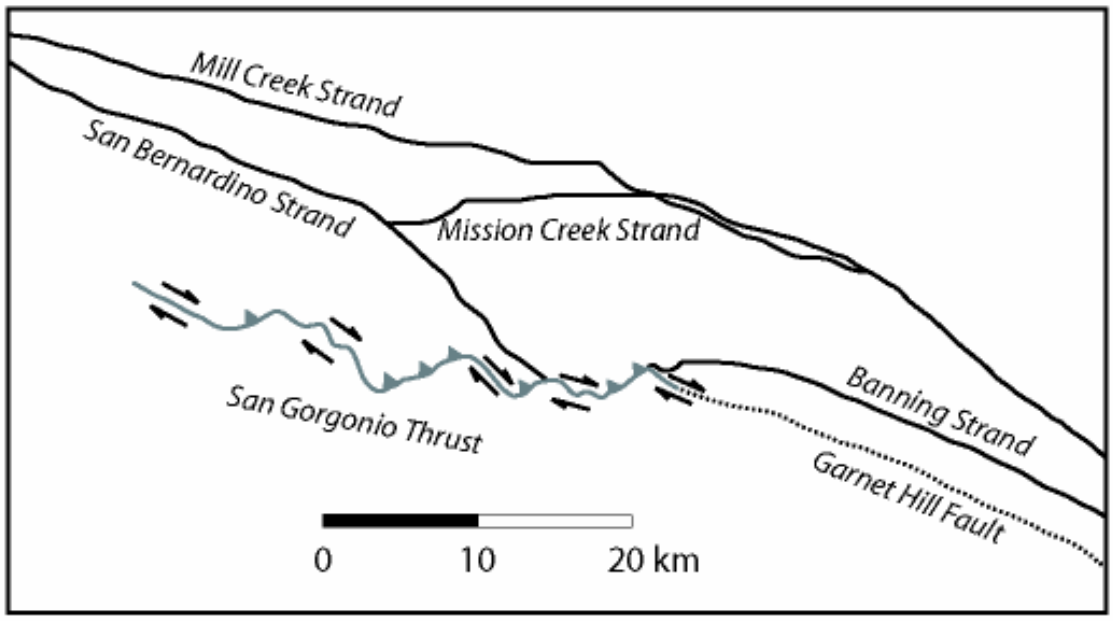

Figure 3.11. Orientation changes of the San Gorgonio thrust surface trace. The saw tooth geometry of the San Gorgonio thrust show in gray. Northwest trending segments of the north-dipping thrust fault favor right lateral strike-slip while the northeast tending segments favor thrusting. The Garnet Hill fault and San Bernardino strand of the San Andreas intersect different right lateral strike-slip favoring segments.

REFERENCES CITED

Allen, C.R., 1957, San Andreas fault zone in the San Gorgonio Pass, southern California: Geological Society of America Bulletin, v. 68, p. 315–350, doi: 10.1130/0016-7606(1957)68[315:SAFZIS]2.0.CO;2.

Anderson, R.S., 1990. Evolution of the northern Santa Cruz Mountains by advection of crust past a San Andreas Fault bend: Science, V. 249, I. 4967, p.397–401.

Behr, W., Hudnut, K., Platt. J., Kendrick, K., Sharp, W., Fletcher K., Finkel, R., and Rood, D., 2007, A revised slip rate estimate for the Mission Creek-Coachella Valley strand of the southern San Andreas fault at Biskra Palms Oasis, Indio, California: Southern California Earthquake Center – Proceedings with Abstracts, v. 17.

Bennett, R.A., Davis, J.L., and Wernicke, B.P., 1999, Present-day pattern of Cordilleran deformation in the western United States: Geology, v. 27, no. 4, p. 371–374, doi: 10.1130/0091-7613(1999)027<0371:PDPOCD>2.3.CO;2.

Bennett, R.A., Friedrich, A.K., and Furlong, K.P., 2004, Codependent histories of the San Andreas and San Jacinto fault zone from inversion of the fault displacement rates: Geology, v. 32, n. 11, p. 961-964, doi: 10.130/G20806.1

Carena, S., Suppe, J., and Kao, H., 2004, Lack of continuity of the San Andreas fault in southern California: Three-dimensional fault models and earthquake scenarios: Journal of Geophysical Research, v. 109, p. B04313, doi: 10.1029/2003JB002643

Clarke, M,M., Harms, K.K., Lienkaemper, J.J., Harwood, D.S., Lajoie, K.R., Matti, J.C., Perkins, J.A., Rymer, M.J., Sarna-Wojcicki, R.V., Sharp, R.V., Sims, J.D., Tinsley, J.C., and Ziony, J.I., 1984, Preliminary slip-rate table for late Quaternary faults of California, US Geologica Survey, Open-File Report, n. 12, p. 84-106.

Crider, J.G., and Pollard, D.D., 1998, Fault linkage: Three-dimensional mechanical interaction between echelon normal faults: Journal of Geophysical Research, v. 103, n. B10, p. 24,373–24,391, doi: 10.1029/98JB01353.

Cooke, M., and Kameda, A., 2002, Mechanical fault interaction within the Los Angeles Basin: A two-dimensional analysis using mechanical efficiency; Journal of Geophysical Research, v. 107, v. B7, doi: 10,1029/2001JB000542.

Cooke, M.L., and Marshall, S.T., 2006, Fault slip rates for three-dimensional models of the Los Angeles metropolitan area, California: Geophysical Research Letters, v. 33, L21313, doi: 10.1029/2006GL027850.

Cooke, M.L., and Murphy, S., 2004, Assessing the work budget and efficiency of fault systems using mechanical models: Journal of Geophysical Research, v. 109, B10408, doi: 10:1029/2004JB002968.

Crouch, S.L., and Starfield, A.M., 1990, *Boundary element methods in solid mechanics: With application in rock mechanics and geologic engineering*: London, Unwin Hyman, 322 p.

Dair, L., and Cooke, M.L., In Press, San Andreas fault geometry through the San Gorgonio Pass, California: Geology.

Del Castello, M., and Cooke, M.L., 2007, Underthrusting-accretion cycle; work budget as revealed by the boundary element method: Journal of Geophysical Research, v. 112, B12, doi: 10.1029/2007JB00497.

Dibblee, T., 1975, Late Quaternary uplift of the San Bernardino Mountains of the San Andreas and related faults: Special Report - California Division of Mines and Geology, v. 118, p. 127–137.

Dokka, R.K., and Travis, C.J., 1990, Late Cenozoic strike-slip faulting in the Mojave Desert, California: Tectonics, v. 9, p. 311-340.

Du, Y., and Aydin, A., 1993, The maximum distortional strain energy density criterion for shear fracture propagation with applications to the growth paths of en echelon faults: Geophysical Research Letters, v. 20, p. 1091-1094.

Gomez, F., Karam, G., Khawlie, M., McClusky, S., Vernant, P., Reilinger, R., Jaafar, R., Tabet, C., Khair, K., and Barazangi, M., 2007, Global Position System measurements of strain accumulation and slip transfer through the restraining bend along the Dead Sea fault system Lebanon: Geophysical Journal International, v. 168, p. 1021-1028, doi:10.1111/j.1365-246X.2006.03328.x.

Griffith, W. A., and Cooke, M.L., 2004, Mechanical validation of the three-dimensional intersection geometry between the Puente Hills blind-thrust system and the Whittier fault, Los Angeles, California: Bulletin of the Seismological Society of America, v. 94, p. 493-505.

_____ 2005, How sensitive are fault slip rates in the Los Angeles to tectonic boundary conditions?: Bulletin of Seismological Society of America, v. 95, p. 1263 – 1275.

Harris, R.A., Archuleta, R.J., and Day, S.M., 1991, Fault steps and dynamic rupture process: 2-d numerical simulations of a spontaneously propagating shear fracture: Geophysical Research Letters, v. 18, p. 893–896, doi: 10.1029/91GL01061.

Jeager, J.C., and Cook, N.G.W., 1976, *Fundamentals of Rock Mechanics*: John Wiley, Hoboken, N.J., 49 p.

Kendrick, K.J., Morton, D.M., Wells, S.G., and Simpson, R.W., 2002, Spatial and temporal deformation along the northern San Jacinto fault, southern California; implications for slip rates: Bulletin of the Seismological Society of America, v. 92, i. 7, p. 2782–2802.

Langenheim, V.E., Jachens, R.C., Matti, J.C., Hauksson, E., Morton, D.M., and Christensen, A., 2005, Geophysical evidence for wedging in the San Gorgonio Pass structural knot, souther San Andreas fault zone, southern California: Geological Society of America Bulletin, v. 117, n. 11/12, p. 1554-1572, doi: 10.1130/B25760.1.

Magistrale H., Day, S., Clayton, R.W., and Graves, R., 2000, The SCEC southern California reference three-dimensional seismic velocity model version 2: Bulletin of the Seismological Society of America 90, p. S65 – S76.

Marshall, S.T., Cooke, M.L., and Owen, S.E., 2008, Effects of nonplanar fault topology on mechanical interaction on fault-slip distributions in the Ventura Basin, California: Bulletin of Seismological Society of America, v. 98, n. 3, p. 1113-1127, doi: 10.1785/0120070159.

Matti, J.C., and Morton, D.M., 1993, Paleographic evolution of the San Andreas fault in Southern California: A reconstruction based on new cross-fault correlation: in Powel, R.E., Weldon, R.J.II, and Matti, J.C., eds., The San Andreas Fault System: Displacement, Palinspastic Reconstruction, and Geologic Evolution: Boulder Colorado, Geological Society of America Memoir 178.

Matti, J.C., Morton, D.M., and Cox, B.F., 1985, Distribution and geologic relations of fault systems in the vicinity of the central Transverse Ranges, southern California: US Geological Survey Open-File Report 85–365, 23 p.

_____ 1992, The San Andreas fault system in the vicinity of the central Transverse Ranges province, southern California: US Geological Survey Open-File Report 92–354, 52 p.

McGill, S., Kendrick, K., and Weldon, R.J., II, and Owen, L., 2007, Pleistocene and Holocene slip rate of the San Andreas fault at Badger Canyon, San Bernardino, California: Southern California Earthquake Center – Proceedings with Abstracts, v. 17.

McGill, S.F., and Sieh, K.E., 1991, Surficial offsets on the central and eastern Garlock fault associated with prehistoric earthquakes: Journal of Geophysical Research, v. 96, p. 21,597-21,621.

_____ 1993, Holocene slip rates of the central Garlock fault in southern Searles Valley, California: Journal of Geophysical Research, v. 98, n. B8, p. 14,217-14,231.

McGill, S., Weldon, R.J.I.I., Kendrick, K., and Owen, L., 2006, Late Pleistocene slip rate of the San Bernardino strand of the San Andreas fault in Highland: possible confirmation of the low rate suggested by geodetic data: Seismological Research Letters, v. 77, no. 2, p. 279.

Meade, B.J., and Hager, B.H., 2005, Block models of crustal motion in southern California constrained by GPS measurements: Journal of Geophysical Research, v. 110, p. B03403, doi: 10.1029/2004JB003209.

Meigs, A.J., Cooke, M.L., and Marshall, S.T., 2008, Using vertical rock uplift patterns to constrain the three-dimensional fault configurations in the Los Angeles Basin: Bulletin of Seismological Society of America, v. 98, n. 2, p. 106-123,doi: 10.1785/0120060254.

Meisling, K.E., 1984, Neotectonics of the north frontal fault system of the San Bernardino Mountains, southern California, Ph.D. Thesis, California Institute of Technology, Pasadena, 394 p.

Morton, D.M., and Matti, J.C., 1993, Extension and contraction within an evolving divergent strike-slip fault complex: the San Andreas and San Jacinto fault zone at their convergence in southern California: *in* Powel, R.E., Weldon, R.J.II, and Matti, J.C., eds., The San Andreas Fault System: Displacement, Palinspastic Reconstruction, and Geologic Evolution: Boulder Colorado, Geological Society of America Memoir 178.

Muller, J.R., and Aydin, A., 2003, Using geomechanical modeling to constrain the 3-D fault geometry within the Marmara Sea, Turkey: Geological Society of America, Abstracts with Programs, v. 35, i. 6, p. 40.

Nicholson, C., 1996, Seismic Behavior of the Southern San Andreas Fault zone in the Northern Coachella Valley, California: comparison of the 1948 and 1986 earthquake sequences: Bulletin of the Seismological Society of America, v. 86, n. 5, p. 1331-1349.

Okubo, C.H., and Schultz, R. A., 2005, Evolution of damage zone geometry and intensity in porous sandstone: Insight gained from strain energy density: Journal of the Geological Society, London, v. 162, p. 939-949.

Olson, E.L., and Cooke, M.L., 2005, Application of three fault growth criteria to the Puente Hills thrust system, Los Angeles, California, USA: Journal of Structural Geology, v. 27, p. 1765-1777, doi: 10.1016/j/jsg.2005.02.005.

Olsen, K.B., Day, S.M., Minster, J.B., Cui, Y., Chourasia, A., Okaya, D., Meachling, P., Jordon, T., 2008, Terashake2; Spontaneous *rupture simulations* of Mw 7.7 earthquakes on the southern San Andreas Fault: Bulletin of the Seismological Society of America, v. 98, i. 3, p. 1162-1185.

Orozco, A.A., 2004, Offset of a mid-Holocene alluvial fan near Banning, CA; constraints on the slip rate of the San Bernardino strand of the San Andreas fault, Master's Thesis, 56 p., University of California at Northridge, Northridge, California.

Oskin, M., and Iriondo, A., 2004, Large-magnitude transient strain accumulation on the Blackwater fault, eastern California shear zone: Geology, v. 32, p. 313-316.

Oskin, M., Perg, L., Shelef, E., Strane, M., Gurney, E., Singer, B., and Zhang, X., 2008, Elevated shear zone loading rate during an earthquake cluster in eastern California: Geology, v. 36, n. 6, p. 507-510.

Plesch, A., and 27 others, 2007, Community fault model (CFM) for southern California: Bulletin of the Seismological Society of America, v. 97, no. 6, p. 1793–1802, doi: 10.1785/0120050211.

Pollard, D.D., Maerten, F., Maerten, L., Resor, P.G., Fiore, P.E., 2002, Forward 3D modeling of complex fault systems using an elastic boundary element method: Geological Society of America, Abstracts with Programs, v. 34, i. 6, p. 251.

Roberts, G.P., and Michetti, A.M., 2004, Spatial and temporal variations in growth rates along active normal fault systems: an example from the Lazio-Abruzzo Apennines, central Italy: Journal of Structural Geology, v. 26, p. 339–376, doi: 10.1016/S0191-8141(03)00103-2.

Rockwell, T., Loughman, C., and Merifield, P., 1990, Late quaternary rate of slip along the San Jacinto fault zone near Anza, southern California: Journal of Geophysical Research, v. 95, B6, p. 8593–8605, doi: 10.1029/JB095iB06p08593.

Shen, Z.K., Agnew, D.C., King, R.W., Dong, D., Herring, T.A., Wang, M., Johnson, H., Anderson, G., Nikolaidis, R., van Domselaar, M., Hudnut, K.W., and Jackson, D.D., 2003, The SCEC crustal motion map, version 3.0: Los Angeles, California, Southern California Earthquake Center.

Sieh, K., Jones, L., Hauksson, E., Hudnut, K., Eberhart-Phillips, D., Heaton, T., Hough, S., Hutton, K., Kanamoi, H., Lilje, A., Lindvall, S., McGill, S., Mori, J., Rubin, C., Spotila, J., Stock, J., Kie Thio, H., Treiman, J., Wernicke, B., Zachariasen, J., 1993, Near-field investigations of the Landers earthquake sequence, April to July 1992: Science, v. 260, p. 171-175.

Smith, B.R., and Sandwell, D.T., 2003, Coulomb stress accumulation along the San Andreas Fault system: Journal of Geophysical Research, v. 108, n. B6, 2296, doi:10.1029/2002JB002136

_____ 2006, A model of the earthquake cycle along the San Andreas Fault System for the last 1000 years: Journal of Geophysical Research, v. 111, p. B01405, doi: 10.1029/2005JB003703.

Spotila, J.A., Farley, K.A., and Sieh, K., 1998, Uplift and erosion of the San Bernardino Mountains associated with transpression along the San Andreas fault, California, as constrained by radio helium thermochronometry: Tectonics, v. 17, n. 3, p. 360-378.

Spotila, J.A., Farley, K.A., Yule, J.D., and Reiners, P.W., 2001, Near-field transpressive deformation along the San Andreas fault zone in southern California, based on exhumation constrained by (U-Th)/He dating: Journal of Geophysical Research, v. 106, n. B12, p. 30909–30922, doi: 10.1029/2001JB000348.

Spotila, J.A., Niemi, N., Brady, R., House, M., and Buscher, J., 2007, Long-term continental deformation associated with transpressive plate motion: The San Andreas fault: Geology, v. 35, no. 11, p. 967–970, doi: 10.1130/G23816A.1.

Spotila, J.A., and Sieh, K., 2000, Architecture of transpressional thrust faulting in the San Bernardino Mountains, southern California, from deformation of a deeply weathered surface: Tectonics, v. 19, no. 4, p. 589–615, doi: 10.1029/1999TC001150.

Thomas, A.L., 1993, POLY3D: A three-dimensional, polygonal element, displacement discontinuity boundary element computer program with applications for fractures, faults, and cavities in the Earth's crust, Master's thesis, 52 p., Stanford University., Stanford, California.

Wald, D.J., and Heaton, T.H., 1994, Spatial and temporal distribution of slip for the Landers, California, earthquake: Bulletin of the Seismological Society of America, v. 84, p. 668–691.

Weldon, R., Fumal, T., Biasi, G., 2004, Wrightwood and the earthquake cycle: what a long recurrence record tells up about how faults work: GSA Today, v. 14, n. 9, doi: 10.1130/1052-5173(2004)014.

Weldon, R., Fumal, T., Biasi, G., and Sharer, K., 2005, Past and Future Earthquakes on the San Andreas Fault: Science, v. 308, p. 966–967, doi: 10.1126/science.1111707.

Weldon, R.J., II, and Sieh, K., 1985, Holocene rate of slip and tentative recurrence interval for large earthquakes on the San Andreas fault, Cajon Pass, southern California: Geological Society of America – Bulletin, v. 96, p. 793–812.

Yule, J., Fumal, T., McGill, S., and Seitz, G., 2001, Active tectonics and paleoseismic record of the San Andreas fault, Wrightwood to Indio: working toward a forecast of the next "Big Event": Geologic Excursions in the Californian Deserts and Adjacent Transverse Ranges, edited by Dunne, G., and Cooper, J., Pacific Section, Society of Economic Paleontologists and Mineralogists, Los Angeles, California, p. 91–126.

Yule, D., Sieh K., 2003, Complexities of the San Andreas fault near San Gorgonio pass: Implications for large earthquakes: Journal of Geophysical Research., v. 109, n. B11, 2548, doi: 10.1029/2001JB000451.